Fluvial landscapes of the Cretaceous: Insights integrating stable isotope
Bachelor of Arts

By

Erica Sarah Janecke. Evans
Colorado College

May 16, 2016

ACKNOWLEDGEMENTS

This thesis was the result of a massive amount of collaboration, and I was fortunate to have the opportunity to work with an amazing group of intelligent and dedicated scientists. I would like to thank Dr. Henry Fricke for advising me on this project and throughout all of college. Thanks to the Denver Museum of Nature and Science for letting me use their collections for sampling- specifically thanks to Drs. Joe Sertich, Ian Miller, Mike Getty and Tyler Lyson for all of their help and advice. This project would not have been possible without the funding of the Keller Venture Grant and Buster Grant. I would also like to thank the labs I had the pleasure of working with- University of Arizona and David Dettman for running my carbonate samples. Thanks to the University of Washington IsoLab, Andrew Schauer, Landon Burgener, and Dr. Katherine Huntington for all of their help with clumped isotopologue work. Additional thanks to Dr. Brady Foreman, Dr. Leif Tapanila and Amy Hudson for sending me samples. Thank you to Texas Petrographics for mounting and making my thin sections. Thanks to Steve Weaver for his technical assistance with the XRD, microscope, and rock saw, and to Dr. Fredrick Tinsley for assistance with statistical analysis. Thanks to the entire Colorado College Geology Department for guiding me and teaching me throughout the last four years. My time here has been invaluable and I cannot imagine college without the support and assistance of this department.

Table of Contents

List of Figures

List of Tables

List of Equations

ABSTRACT

This project is focused on the study of climate, hydrology, and surface processes of western North America during the late Cretaceous (~75 million years ago) in what is now southern Utah. The goal of this project is to describe in detail the hydrology of fluvial systems associated with the deposition of the Kaiparowits Formation. Differences in stable isotope ratios of gar ganoine, pedogenic carbonate, and enamel from hadrosaur and crocodile teeth, in conjunction with previously published bivalve data, indicate there are three main parts to the fluvial system: 1) FS1—large anastomosing rivers draining upland areas 2) FS2—lakes subject to episodic flooding and 3) FS3—smaller streams draining the foreland basin. Furthermore, it is possible to infer mixing of water between these sources, in particular the mixing of FS1 and FS3 waters to form FS2 water, presumably during seasonal flooding events that were analogous to processes taking place in modern-day Tonle Sap Lake in central Cambodia.

The organic content of sediment, carbon isotope ratios of paleosol carbonate, and the carbon isotope ratios of hadrosaur dentine and enamel from different sites all indicate that soils along the margin of the FS2 lakes were characterized by episodic flooding and saturation, with those closer to the margin being saturated for a longer period of time, compared to more distal localities. Furthermore, hadrosaurs that ate vegetation located closer to the lake margin have teeth with high carbon isotope ratios, consistent with the existence of closed canopy forests in these localities. Thus, variations in the hydrology of these fluvial systems appears to have played an important role in determining the distribution of plants over Kaiparowits landscapes, with closed canopy forests perhaps accounting for the large diversity in herbivorous dinosaurs observed in southern Utah during the late Cretaceous.

1. INTRODUCTION

During the Late Cretaceous, western North America was separated from the eastern landmass of Appalachia by the Western Interior Seaway (WIS) (Figure 1). The structural, topographic and sedimentological characteristics of the western landmass, known as Laramidia, were largely influenced by the subduction of the Farallon plate beneath the North American plate. This subduction resulted in the formation of a magmatic arc, and fold and thrust belt similar to the modern Andes Mountains in geologic structure and in elevation (Sewall and Fricke, 2013; Sewall and Sloan, 2006). Areas to the east of this orogenic belt underwent subsidence to form narrow foreland basins that bordered the WIS (DeCelles and Giles, 1996).

The area of focus for this study is the Kaiparowits foreland basin along the southwestern margin of the WIS, in what is now southern Utah. This basin was filled by a thick package of fluvial sediment during the Campanian epoch of the Cretaceous, and is now represented by the Kaiparowits Formation. Most most outcrops of this formation occur in the Grand Staircase Escalante National Monument (GSENM) (Figure 2). The Kaiparowits Formation is comprised of greenish-gray sandstone, mudstone and siltstone eroded into badlands topography (Figure 3a & 3b). The fine-grained nature of the strata, in conjunction with non-marine fauna suggests a low relief plain setting as the environment of deposition (Titus et al., 2013). Hydromorphic paleosols, paludal deposits, presence of aquatic flora and fauna, and large channels indicate that this plain was frequently inundated (Roberts, 2007). Roberts (2007) detailed the variations in eight lithofacies and ancient depositional environments throughout the section, categorizing sandy channel deposits, and overbank mudstone and siltstone as the dominant

Figure 1: Late Cretaceous of North America. A) Dinosaur Park Formation, Alberta; B) Two Medicine Formation, Montana; C) Judith River Formation, Montana; D) Hell Creek Formation, Montana, North and South Dakota; E) Kaiparowits Formation, Utah; F) Fruitland and Kirkland Formations, New Mexico; G) Aguja Formation, Texas. Adapted from Ron Blakey, Colorado Plateau Geosystems.

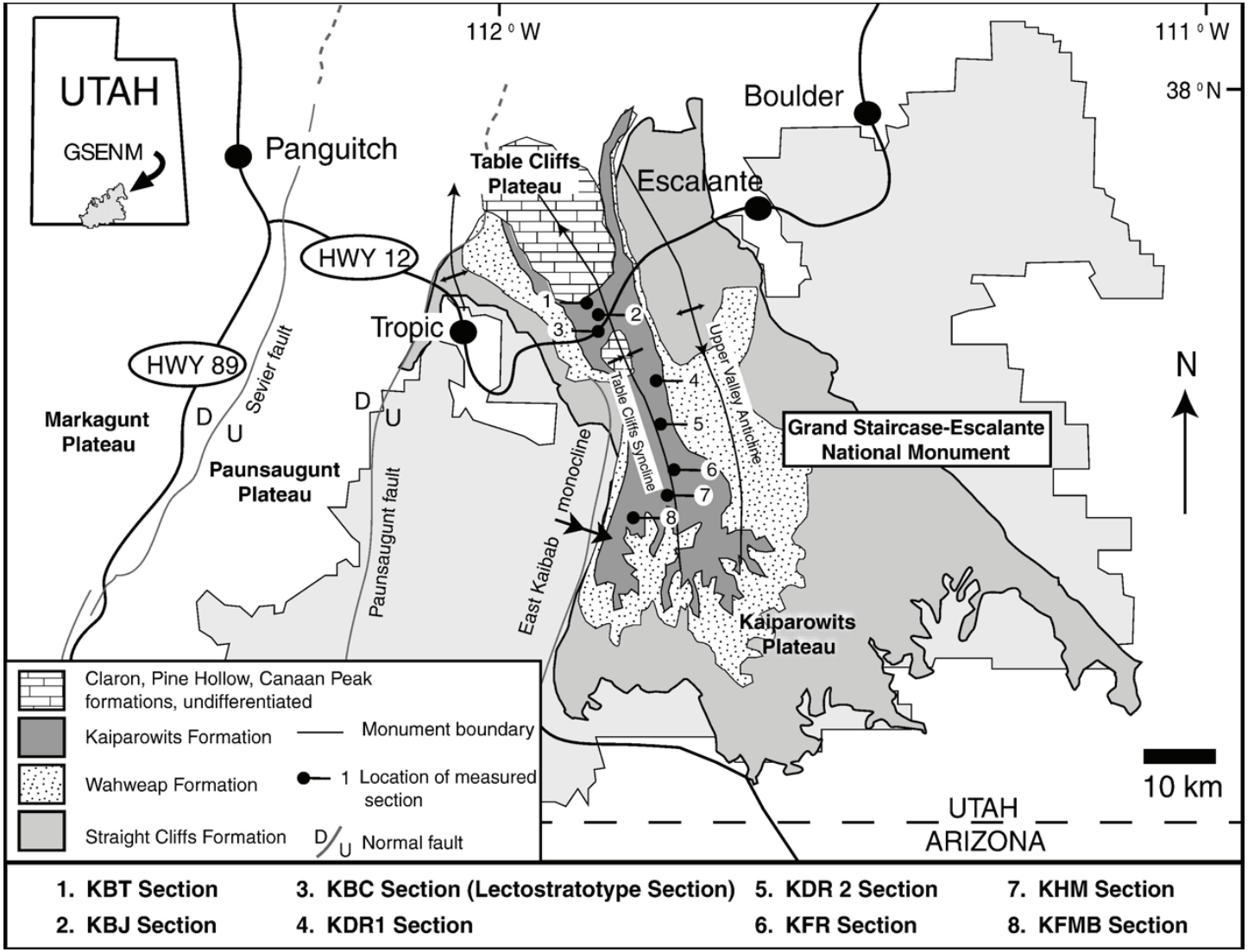

Figure 2: Schematic of the GSENM. Generalized field area and geology. Sections of study are indicated by numbers. Figure from Roberts (2007)

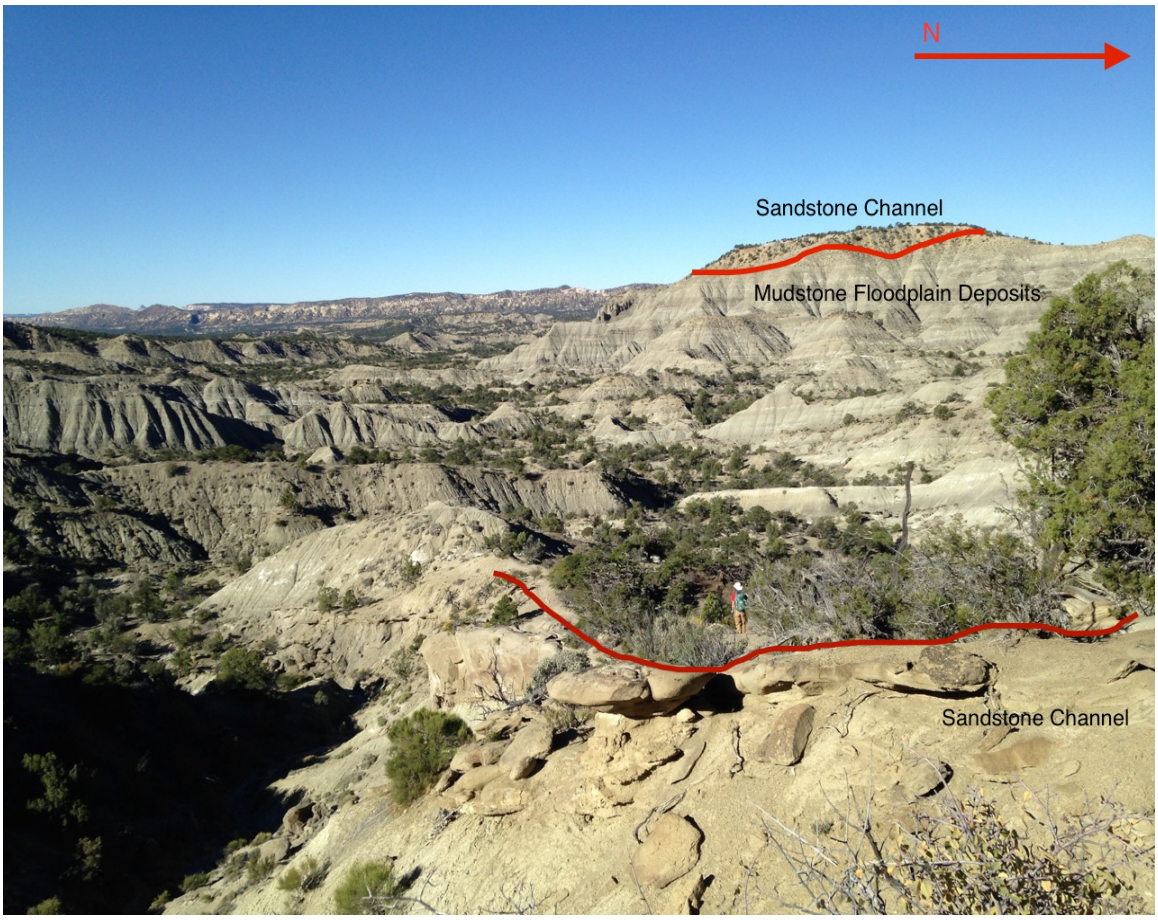

Figure 3a: Field Sites. Top, view looking west into the Fossil Ridge basin. Resistant sandstone channels cap less resistant floodplain mudstones and siltstones. Bottom, looking east from the top of 4362. People in bottom of image are on fossil-producing layer. Small sand lenses can be seen in the lower portion of the image.

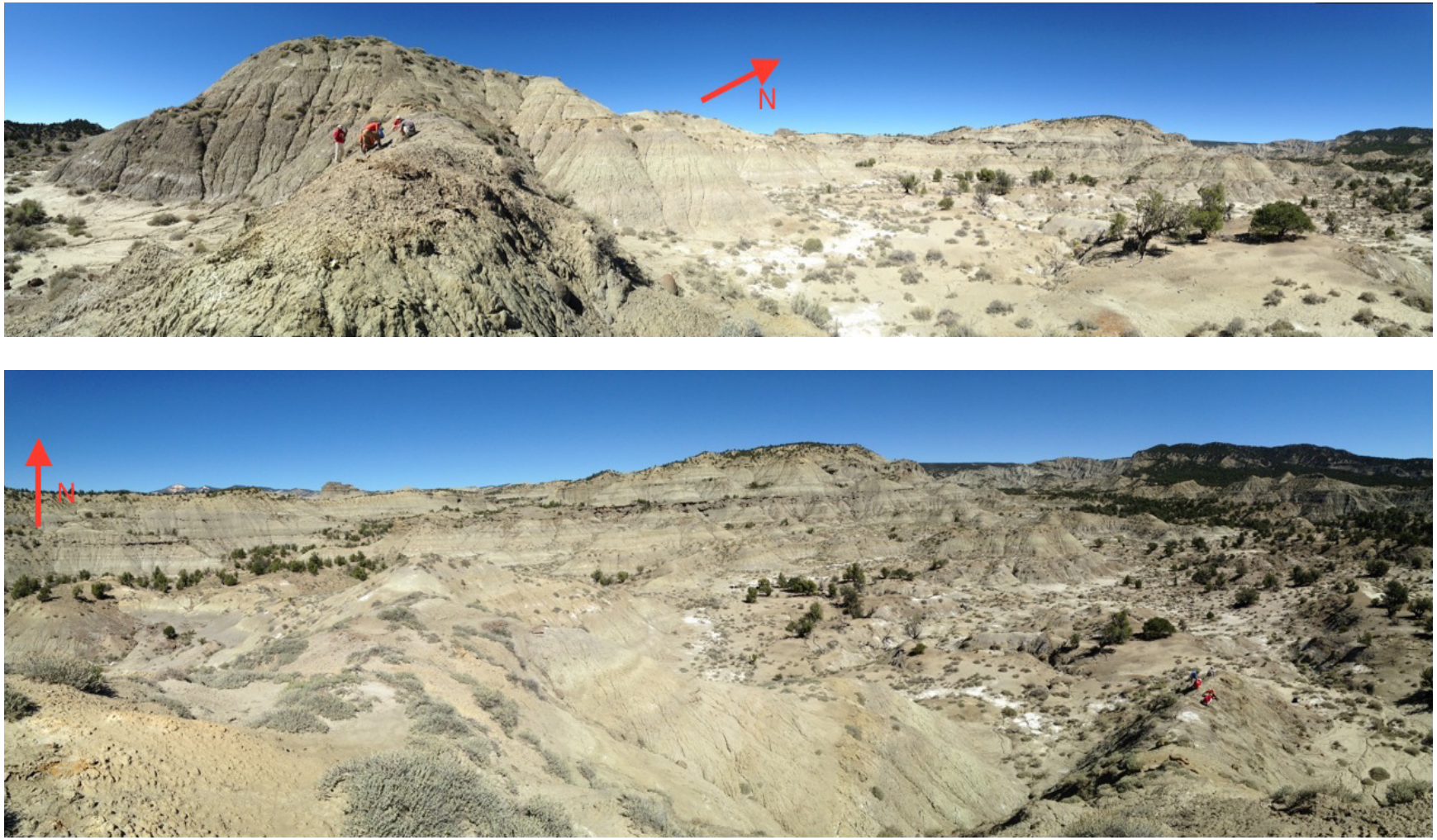

Figure 3b: Field Sites. Top, looking west towards site 4362. Sandstone channels cap hills to the north, and dark mudstone layers with fossil material in the foreground of the image. Bottom, looking to the north from point labeled as “Camp” in Figure 4.

litholofacies throughout the section. Stratigraphically, the formation records changes in sea level, uplift and shifts between meandering and anastomosing river systems (Roberts, 2007; Foreman et al., 2015).

During the Late Cretaceous, the climate of this area was characterized by relatively high mean annual temperatures of ~22°C (Miller et al., 2013), while precipitation was higher than modern (~1.8 meters per year) (Sewall and Fricke, 2013). Global climate model simulations and stable isotope data from fluvial bivalves suggest that precipitation falling in the basin and adjacent highlands was monsoonal (i.e. seasonal) in nature, with the majority of precipitation (77%) falling in summer months (Fricke et al., 2010; Foreman et al., 2015). During this time of the year southeasterly winds rich in moisture moved off the WIS across the foreland basin towards the highlands to the west. This circulation pattern would have been reversed during the drier winter months, with moisture-poor air masses moving westward across the basin.

Fluvial environments of the Kaiparowits Basin were host to to a wide variety of plants and animals. Coniferous gymnosperms, cycads, gingkoes and newly evolved angiosperms (flowering plants) covered the raised interfluves between waterways. Interestingly, vines are common in fossil plant assemblages, which suggest the presence of tall trees that lived close together (Miller, personal communication, 2014). A recent study by Crystal (2014) indicates that there may have been some differences in forest structure over the landscape, with some areas having more of a 'closed-canopy' structure, and others being more open in nature. Living in these forests were at least three coeval taxa of herbivorous Ceratopsids, including *Diabloceratops eatoni, Utahceratops gettyi* and *Kosmoceratops richardsoni* (Loewen et al., 2013). Hadrosaurids (*Parasaurolophus*

and *Gryposaurus)* are also commonly found (Gates et al., 2013). Pachycephalosaurids and Ankylosaurs are less common, but present (Evans et al., 2013; Loewen et al., 2013). Carnivores include a minimum of five taxa of small theropods including oviraptorosaruians, therizinosaurids and tyrannosaurids. In addition to these terrestrial dinosaurs, fossils of semi-aquatic to aquatic reptiles such as crocodiles, turtles, and fish (e.g. gar) are abundant in overbank and pond deposits across the formation (Roberts et al., 2013, Irmis et al., 2013). The diversity and abundance of these fossils indicates that a complex set of ecological relationships existed among plants and animals living in these paleoenvironments.

While it is clear that fluvial sedimentation took place in the Kaiparowits basin under the influence of monsoonal precipitation, and that this seasonal precipitation resulted in the periodic inundation of the landscape, many details regarding the types of water bodies occupying the landscape, and their hydrologic nature (e.g., flow and recharge characteristics) remain unknown. In their stable isotope study of fluvial bivalves, Foreman et al., (2015) suggest that the largest rivers were recharged by high-elevation precipitation falling to the west, while standing water (i.e., ponds or wetlands) located between river channels was recharged by the overbank flooding of these rivers, combined with local precipitation. These authors do not, however, discuss the relationship of this flooding to monsoonal rainfall, the possibility of other types of water bodies on the landscape, or the hydrology of the landscape where there was no standing water. No other paleohydrological research has been published for the Kaiparowits Formation. Thus, the primary goal of this project is to provide a detailed description of hydrological and climatological variations over these coastal plain landscapes. This was

done by measuring the oxygen isotope ratios of a number of different biogenic and authigenic carbonate samples collected from different depositional settings, which are used to infer the isotope ratios of ancient surface water. In addition, hydrological reconstructions made as part of this project are used to infer where closed and open canopy forests were located on the landscape.

2. BACKGROUND

2.1 Stable isotope ratios and surface processes

Stable isotope ratios of earth materials can be used to study paleohydrology, canopy and landscape surface processes because fractionation takes place as oxygen and carbon cycle through earth's reservoirs. Thus, ratios of oxygen and carbon in these materials reflect the conditions of formation. Specific examples relevant to this study are described below.

2.1.1 Oxygen isotope ratios of surface water

As air masses move up over topographic highs and across land, the heavier isotope of oxygen (^{18}O) is removed from the system. This gives rivers that recharge from the highlands a higher $\delta^{18}O$ signature in comparison to rivers that recharge on the floodplains (Foreman et al., 2015). There is also mixing that occurs in the floodplain between rainout precipitation and local water, adding variability to the oxygen isotope across the landscape. The oxygen isotope domains of an area can be expressed through oxygen isotope ratios found in bivalves, fish, and the teeth of aquatic animals (Fricke, 2007).

2.1.2 Carbon isotope ratios of plants and soils

The Mesozoic was dominated by C_3 plants, which preferentially incorporate ^{12}C during photosynthesis, resulting in $\delta^{13}C$ values of ~ 26‰ (Fricke et al., 2008). This ratio is not constant across a landscape, as plants will alter degrees of fractionation as a result of light availability, nutrients, water, salinity, and temperature. Plants that are 'water-stressed' will close their stomata, holding CO_2 in the leaf and preventing gas exchange (Fricke, 2007). This means that plants existing in unfavorable conditions will have more

positive $\delta^{13}C$ values because there is less discrimination in their photosynthetic process (Kohn and Cerling, 2002: Fricke et al., 2009). It is difficult to directly measure the $\delta^{13}C$ values across a landscape as plants are generally not preserved in their original state. However, ratios preserved in soil carbonates and dentine will be reflective of the fractionation occurring in plants and in soils.

Leaf and organic matter is an important part of soil formation, and the breakdown of organic matter results in distinct isotopic signatures. Dry, well-drained soils have lower $\delta^{13}C$ values compared to everwet areas because oxygen is present to react with organic matter to produce CO_2 and H_2O. The breakdown of organic material in the presence of oxygen occurs by oxidation following the pathway of:

$$CH_2O + O_2 \rightarrow CO_2 + H_2O \qquad \text{EQ. 1}$$

This breakdown does not impart a fractionation, and therefore the ratio expressed in this CO_2 is representative of the isotopic ratios of the original organic material. CO_2 produced through the oxidation of organic matter can be incorporated into pedogenic carbonate, or secondary calcite precipitating into tooth dentine. These secondary carbonates are imparted with a fractionation as a result of kinetic molecule motion (Koch, 1998). The carbon isotope fractionation produced by this process is typically in the range of $\delta^{13}C$ of -30‰ to -20‰, in tooth dentine. Calcite precipitation imparts a fractionation of +14‰.

Soil zones that are 'everwet' are more likely to experience methane production, which results in an elevated $\delta^{13}C$ value. This occurs in anoxic soils where bacteria

decompose organic material to produce methane and carbon dioxide (Beerling et al., 2009; Jahren et al., 2004). Methanogens break down carbon in the following manner:

$$CH_3COOH \rightarrow CH_4 + CO_2 \qquad \text{EQ. 2}$$

This processes results in a fractionation of the carbon isotope because methanogens preferentially incorporate ^{12}C over ^{13}C during the production of CH_4 as a result of the kinetic isotope effect for carbon, giving it a very low $\delta^{13}C$ ratio (-110‰ to -50‰) (Whiticar, 1999). Methane then escapes into the atmosphere, removing ^{12}C isotopes from the system. The remaining carbon in the system is therefore enriched in the heavy isotope of carbon. CO_2 produced in this system will have high $\delta^{13}C$ values. In a closed canopy system, this ^{13}C-enriched CO_2 becomes trapped and subsequently recycled, pushing the $\delta^{13}C$ ratio of the soils towards +10‰ to +15‰ (Whiticar, 1999). The presence of variable conditions of organic matter breakdown can be a result of a variety of factors, the most likely being water content of soils, and the presence of a canopy-like forest structure.

2.2 Proxies for ancient surface conditions in biogenic material

Ancient water and organic matter are not preserved directly. Rather, isotope ratios of animals reflect the water they drink and the food they eat. Isotope ratios of these materials are inferred using the isotope ratios of the minerals formed from them. The biogenic material used in this study consists of bivalve shells, gar ganoine, tooth enamel and dentine.

In tooth enamel and dentine, the primary mineral is apatite, $Ca_5(PO_4, CO_3)_3(OH, CO_3)$. Carbon found in the carbonate phase of bioapatite reflects the ratio of carbon in plants consumed by an animal. Oxygen in bioapatite is derived from atmospheric oxygen and ingested water (Fricke et al., 2009). Since the oxygen isotope ratio of the atmosphere has remained relatively constant throughout earth's history, differences in oxygen isotopic ratios in bioapatite of vertebrates should reflect variations in surface water chemistries.

Ganoine is a mineralized tissue, and is formed of rod-shaped apatite crystals (therefore having the formula $Ca_5(PO_4, CO_3)_3(OH, CO_3)$). The carbon in the carbonate phase of ganoine is a reflection of the carbon ingested by gar and therefore reflects carbon present in the waterways in the form of dissolved organic carbon and plant matter. The oxygen ratios present in in ganoine is reflective of the oxygen from the water in which the animals were residing.

Shell material from invertebrates consists of aragonite ($CaCO_3$), and replacement calcite. Calcite is fluvial organisms can be secondary, and therefore shells that were dominantly calcite were not used in this study (see methods section). The ratios of oxygen isotopes in invertebrate material is reflective of of the oxygen isotope ratio of the water they live in. Aragonititic shell material does not undergo a temperature fractionation during production, and therefore unaltered bivalve shells are directly representative of the chemistry of the water they formed in. Temperature formation of bivalves is thought to be limited to 12—25°C, although factors such as ion availability and salinity do come into play (Dettman et al., 1998).

2.3 Authigenic carbonate as proxies for surface conditions

Inorganic carbonate is found in the form of $CaCO_3$ which forms in soils. This inorganic carbonate is often referred to as authigenic or pedogenic carbonate. Oxygen in pedogenic carbonate comes from soil water, while carbon is sourced from soil CO_2, the ratio of which is a product of biologic processes in soils, such as plant root and microbial respiration (Peters et al., 2013). This production source for CO_2 means that $\delta^{13}C$ values in soils will be depleted in the heavy isotope of carbon relative to the rest of the atmosphere. Therefore, carbonate that forms closer to the surface will have more positive $\delta^{13}C$ values when compared to carbonate that precipitated lower in the soil profile (Peters et al., 2013; Cerling & Quade 1993). For this project, soil nodules representative of soil water, and micrites representative of ponded water were collected.

The $\delta^{18}O$ value found in soil carbonate is therefore a function of the chemistry of soil water, and temperature-dependent oxygen-isotope fractionation occurring during formation of carbonate (Kim & O'Neil, 1997; Peters et al., 2013). If a soil is well drained, the precipitation will be the source of soil water (Peters et al., 2013). However, in wetter, more humid environments where soils are not as well drained, soil waters will reflect mixing of surface and standing water chemistry. Carbonate precipitation and resulting isotopic composition of carbonate is a result of a combination of soil moisture, temperature, and pCO2. These factors vary on daily, seasonal and annual scales (Peters et al., 2013). Studies have indicated that temperatures of soil carbonate formation may be warmer than mean annual air temperatures (MAAT) (Peters et al., 2013). Carbonate forms during the summer season (Peters et al., 2013), and therefore these are a strong warm season bias in carbonate isotopic content (Quade et al., 2011).

Dentine found in animal teeth can also be used to make inferences about processes occurring in soils. Apatite makes up the tooth dentine of vertebrates. This dentine has a smaller crystal size than the apatite found in enamel, and is therefore subject to alteration via mineral replacement. The isotopic ratios in dentine are distinct because of this, and are reflective of the soils in which the tooth underwent diagenesis (Fricke et al., 2008; Fricke et al., 2009). Carbon will be indicative of soil processes and the breakdown of organic matter, such as methanogenesis and simple oxidation of organics. Oxygen isotope ratios will be indicative of the water chemistry of soils in which teeth undergo diagenesis.

2.4 Clumped isotopologue thermometry application

Clumped isotopologue thermometry relies on the temperature dependent distribution of heavy and light isotopes in a carbonate material (Chivas and Dux, 2015; Eiler, 2007). Thermodynamic principles indicate that heavier isotopes have a lower zero-point energy and are therefore prefer to bond with each other in molecular structure at lower temperatures. These relationships between isotopes become more stochastic at high temperatures, which means a linear relationship between measured Δ47 value and temperature can be derived (Eiler, 2007). This Δ47 values is a measure of preferential grouping, or "clumping" in a carbonate molecule. Using clumped isotope temperature for carbonates alongside $\delta^{18}O$ of carbonates, it is possible to estimate the $\delta^{18}O$ of formation water for carbonate minerals. For this study, clumped isotope analyses of authigenic soil carbonates and of calcite cements were undertaken in order to study 1) soil temperatures and $\delta^{18}O$ of soil water and 2) burial temperatures.

3. METHODS

3.1 Geologic setting and sample collection

This project focuses on one of the richest Cretaceous vertebrate fossil localities in the world, which due to the remote and rugged terrain is still being actively studied. In particular, The Denver Museum of Nature and Science (DMNS) conducts fieldwork in the Kaiparowits annually for 4-6 weeks, and this project was done in collaboration with museum scientists. The majority of samples were collected from or near sites along "Fossil Ridge" where vertebrate fossils are located. The Fossil Ridge field area exposes the lower and middle members, while the sites sampled in this thesis are located in the lower third of the middle member (Sertich and Miller, personal communication, 2014). Units within GSENM are dipping gently to the north, and the dip increases towards the base of the unit making correlation difficult. However, alluvial architecture and ash bed dating methods can be used to broadly determine age and stratigraphic position of field sites (Roberts, 2007). The materials sampled in the project are representative of the 'overbank' facies described in Roberts (2007) (facies 8 and 9), and are broadly representative of anastomosing channels and overbank sediment deposits located at ~450 m in stratigraphic position in section. The goal of this sampling was to collect material from a single horizon. This was accomplished by walking along contacts and tracing out beds between sites (see Figure 4). Overall, sites are no more than ten meters apart in height, and arrayed over an area ~3 km^2, with the exception of the V108/KS-20 and 4445. The 4445 site is located within the study area, but is about 10-15m up in section. Similarly, V108/KS-20 contains material from an area known as "The Blues" which is positioned in the upper third of the formation. From each site a suite of materials was

collected. On the biogenic front, hadrosaur teeth, crocodile teeth, bivalves and gar scales were collected. Authigenic carbonate in the form of carbonate pond deposits, cements and nodules were also collected. Table 1 presents lithology and material collected from each site. Bulk isotopic analyses were run in the summer of 2015, clumped isotopic analysis was done during the fall of 2015.

Map of Fossil Ridge Field Sites

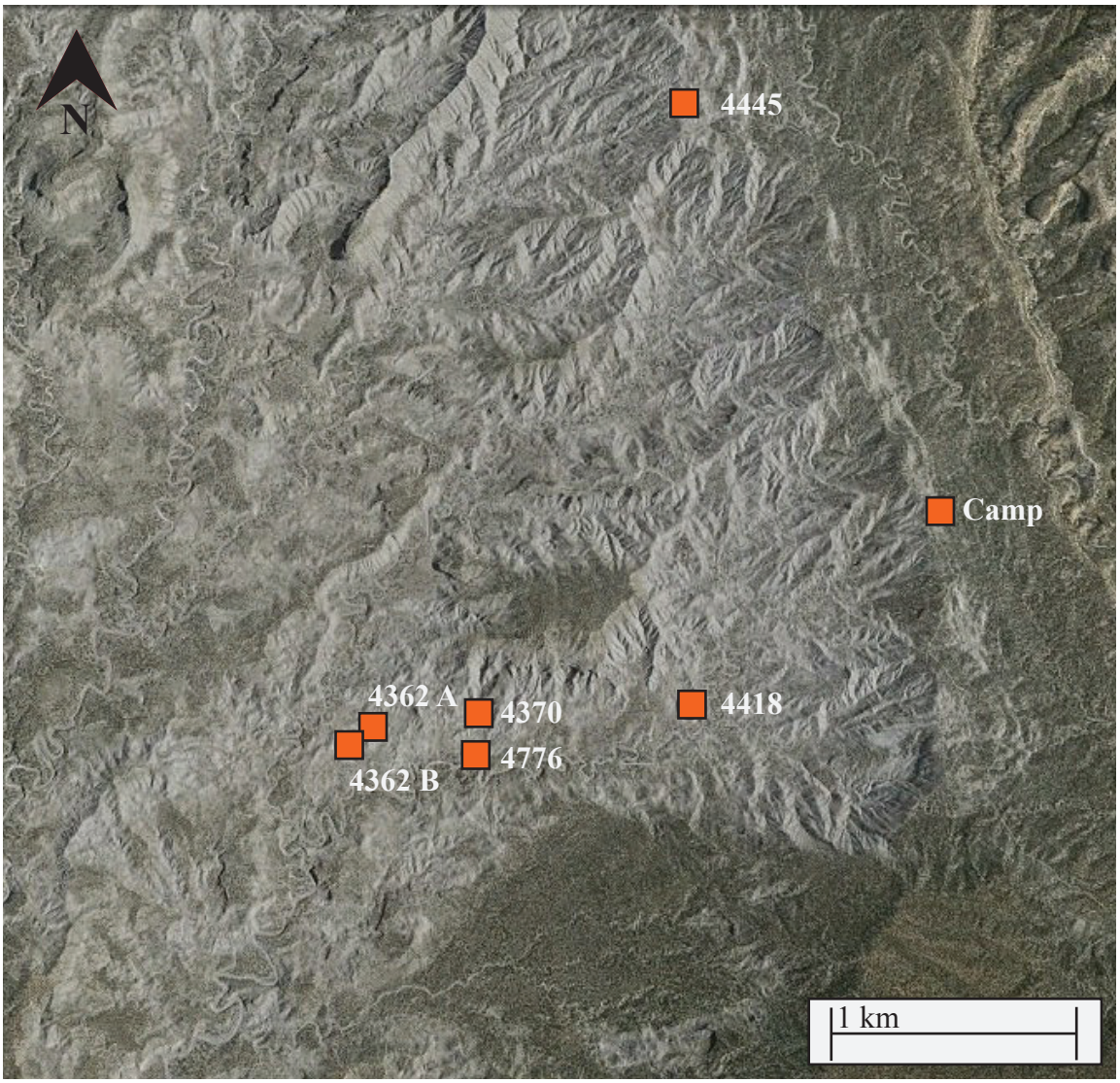

Figure 4: Map of Fossil Ridge field sites collected for this study. V108/KS-20 are located ~20 km to the northwest and up section. Collection materials from sites contain paleosols, vertebrate material (teeth and scales), nodules and micrite beds (when present). site 4362 is a very productive layer that is laterally extensive and crops up in several areas. Horizon A and horizon B have both been collected by DMNS and produce a large number of fossils. Site 4362 is also associated with adjacent micrite beds and nodule layers below the fossil horizon.

NAME	DMNS #	LITHOLOGY	FOSSILS	FACIES (Roberts, 2007)
FOSSIL RIDGE				
Microsite Mecca	KPS 12180, 4362	Dark grey mudstone layer, nodule beds down section, adjacent micrites	Hadrosaur teeth, gar scales, crocodile teeth, invertebrate material	FA8- floodplain ponds and lakes
Two Teeth	KPS 13084, 13030, 4370	Dark grey mudstone, in situ carbonate nodules	Hadrosaur teeth, gar scales, invertebrate material	FA8- floodplain ponds and lakes
4418	KPS 11029, 4418	Medium grey silty mudstone	Hadrosaur teeth	FA8- floodplain ponds and lakes
Turtle Town	KPS 13084, 13030 DMNS 4776/4778	Medium-light grey mudstone	Hadrosaur teeth, gar scales, invertebrate material	FA8- floodplain ponds and lakes
NORTH OF FOSSIL RIDGE				
Pistachio Hills	4445	Green-light grey silty mudstone carbonate pools, nodules	Hadrosaur teeth, gar scales, invertebrate material	FA8- floodplain ponds and lakes
THE BLUES				
V108/KS-20	UT 14426	Green/grey silty mudstone	Hadrosaur teeth, gar scales, invertebrate material	FA8- floodplain ponds and lakes

Table 1: Field sites.

3.2 Analytical methods and mineralogical identification

Paleosol nodules were sliced on the Colorado College rock saw, rinsed and washed. Cut surfaces were inspected for feldspar crystal inclusions indicative of alteration. Samples were powdered on a diamond tipped dremel drill at low speeds from central unaltered sections of nodules and bivalves. Bivalves were cleaned, and powdered from unaltered sections (fifty milligrams of bivalve material from each bulk rock was powdered for bulk mineral analysis using X-Ray diffractometery). Dentine and enamel were sampled from teeth, while ganoine was sampled from gar scales. Sandy carbonate cements were drilled with the Colorado College standing drill. Tooth enamel, gar ganoine and dentine were soaked in 0.1M acetic acid, then rinsed and centrifuged three times to remove secondary carbonate (Kohn & Cerling, 2002). These samples were then baked at 40°C for 24-48 hours. Carbon and oxygen isotope ratios were obtained at the University of Arizona on a KIEL-III carbonate preparation device coupled with a Finnegan MAT 252 mass spectrometer. Powdered samples of bivalves, teeth, scales and nodules were weighed on silver foil and reacted with phosphoric acid (H_3PO_4) at 70°C within a vacuum. CO_2 and H_2O released from this reaction were then captured into a small volume cold finger trap held at -196°C. This is then warmed, allowing CO_2 to pass into the Finnigan mass spectrometer through a capillary for mass charge measurements. Stable isotope ratios are reported as $\delta^{13}C$ and $\delta^{18}O$ values, where:

$$\delta = (R_{sample}/R_{standard} - 1)*1000\ ‰ \qquad \text{EQ. 3}$$

and the standard is VPDB for both carbon and oxygen. The isotope ratio measurement is calibrated based on repeated measurements of NBS-19, NBS-18, and in-house powdered carbonate standards. Analytical precision is ± 0.1 ‰ for both $\delta^{18}O$ and $\delta^{13}C$ (1σ). The carbonate – CO_2 fractionation for the acid extraction is assumed to be identical to calcite. Paleosol soils were also analyzed for bulk organic composition, which is related to rock color in Figure 5.

3.3 Clumped isotope analysis

Clumped isotope analysis was incorporated into this project in an attempt to eliminate variability when estimating the oxygen isotopic ratios of meteoritic water. Samples were selected for clumped isotope thermometry based on their isotopic values similar to other materials collected in this study, their calcite contents as well as stratigraphic proximity to sites of interest. Bivalves and adjacent cements that did not display secondary calcite replacement were also selected for this sampling, in an attempt to derive water temperatures. Materials were first prepared in the same way as described for carbon and oxygen isotope ratios. Then they were analyzed in the University of Washington Isolab, using a KIEL-III carbonate preparation machine to determine percent carbonate. This value is needed to determine the mass of material needed for the clumped isotope analysis. Eight to ten milligrams of powder were then weighed and digested in a bath of phosphoric acid (H_3PO_4) at 90°C to produce CO_2. This was then cryogenically separated from water along a stainless steel vacuum line, at the end of which purified CO_2 was transferred to a Pyrex break seal. These break seals were then placed in a Thermo MAT253 mass spectrometer and analyzed along with a daily standard (CCO4, C2, CORAL, ETH2 and CCO40). Data were reduced and processed in Microsoft Excel

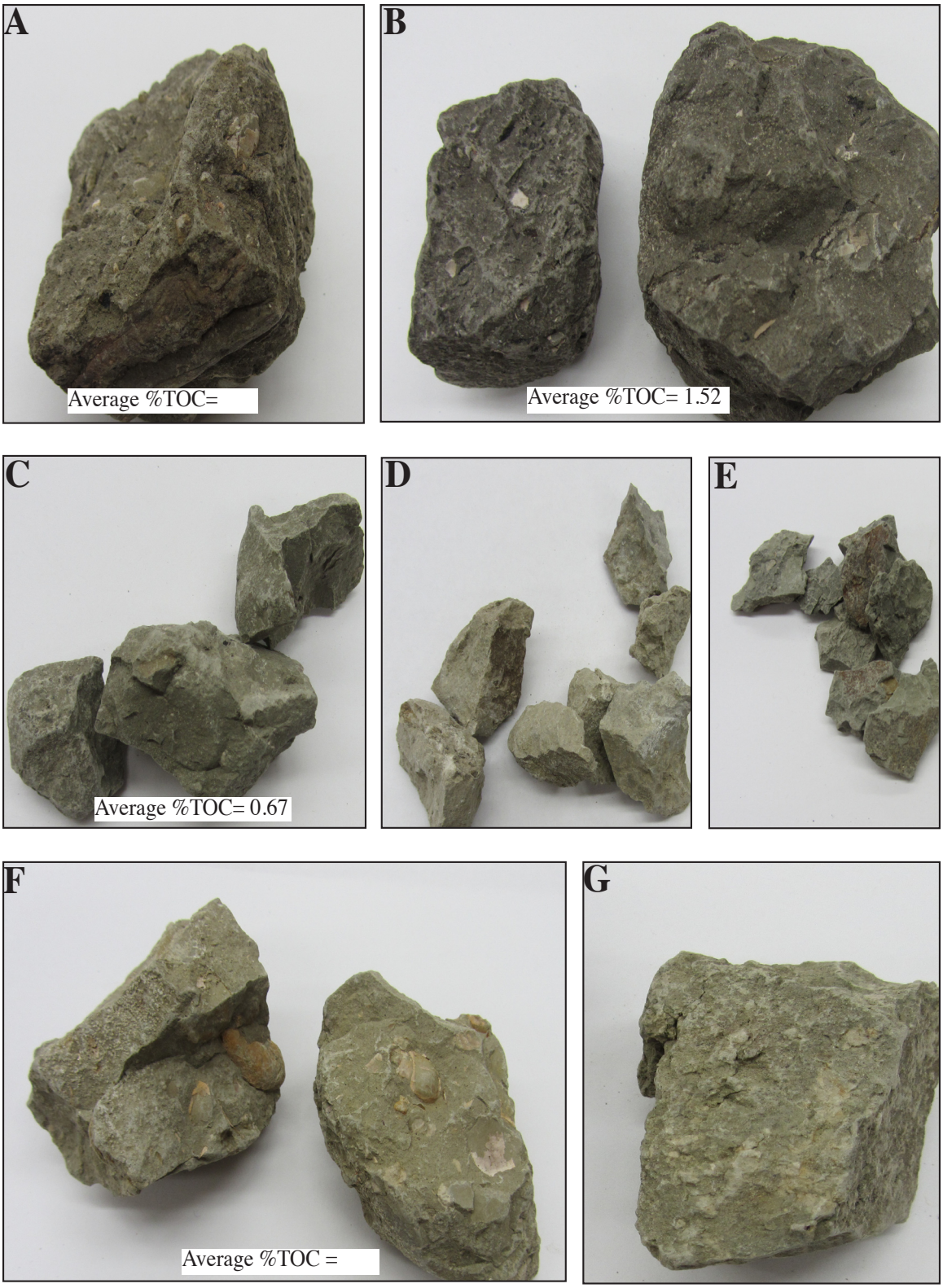

Figure 5: Mudstone color changes. Relative color changes in mudstone samples used in this study a) 4362 west b) 4370 c) 4418 d) 4362 east e) 4776 f) V108/KS-20 g) 4445. All rocks are handsample size. A and B represent the most carbon-rich end of the specturm, C-E are the more intermediate members, and F-G are the least carbon-rich, representing more upland, drier and less aquatic sites.%TOC presented when data are available.

and in MAT lab, using the scripts 'polly' and 'pollycompile', written by Andrew Schauer at the University of Washington. Δ47 values were computed through MATlab, and temperatures were calculated using the equations determined by Kluge et al. (2015) and Zaaur (2013). Methods used for preparation and analyses are most similar to those outlined by Kluge et al. (2015). Meteoric water chemistry was then calculated from temperature using equations outlined in Kim & O'Neil (1997).

Within the preparation method described (Kluge et al., 2015) there is a secondary fractionation that occurs during the breakdown of $CaCO_3$ with H_3PO_4. When calcium carbonate reacts with acid, two oxygen atoms are liberated into CO_2, while one remains in H_2O. This means that there will not be a random distribution of isotopes of oxygen present in the CO_2 gas produced for analysis. Repeated experiments of synthetic carbonate dissolution (Kluge et al., 2015; Zaarur, 2013) have derived acid fractionation factors for a range of temperatures. The methods described by Kluge et al. (2015) are most similar to this laboratory procedure, and the derived relationship between Δ47 and temperature in the Kluge et al. (2015) model accounts for the acid fractionation at 90°C. Therefore, the equation used for this data is:

$$\Delta 47 = \frac{0.362(\pm 0.018) * 10^5}{T^2} + 0.292(\pm 0.019) \qquad \text{EQ. 4 (Kluge et al., 2015)}$$

Due to the small mass differential measured in clumped isotope mass spectrometry, there is a degree of error and variability inherent and possible from comparisons between labs. In order to eliminate this differential, data produced at the University of Washington were converted to the absolute reference frame proposed by

Dennis et al. (2011). This reference frame compares lab-derived values for known reference gases heated at specific temperatures (4°C, 60°C, and 1000°C) versus theoretical Δ47 values. Standard values are run repeatedly and are averaged together to reduce the standard deviation of measurements, and to generate a linear regression equation to correct data produced in the lab back to the standard. Corrections can then be applied to data to account for lab variability (temperature, pressure, humidity, equipment, etc.) (Huntington et al., 2009). This correction was done in MATLAB, using a script written by Andrew Schauer at the University of Washington.

3.4 Thin section analysis

Although nodules analyzed for this study did not appear to have alteration upon cursory inspection of clean cut surfaces, high Δ47 temperatures in some sample sets seems to indicate that alternation may have occurred in these samples. In order to quantify the degree of this alteration, thin sections were made by mounting slices of nodule in clear gel at Texas Petrographic Laboratory in Houston Texas. Images of sections were taken on the Leticia microscope at Colorado College, as well as the Leticia and whole section scopes at Utah State University. These section images were analyzed in the program ImageJ. Pictures were taken of whole nodules and cement complexes, as well as a representative sample of internal nodule structures, such as altered edges and veins. Because there is a large size difference between micritic carbonate and altered spar-rich granular carbonate, analyses were based on particle size. Image color spectrums were altered, and converted into binary black and white images. ImageJ then totaled area size of particles greater than 0.004μm. A cut off area of .004μm was chosen because it is generally thought to be the boundary between fine carbonate muds and secondary crystal

growth. Images were also taken with the entire field of view to capture whole nodules. These images were trimmed in Photoshop to remove backgrounds, and exported in TIFF format so that ImageJ could calculate alteration area for the nodule alone. Structures within nodules were classified and grouped into centers, edges, veins, and large vug crystal ingrowths. Images were then taken of specific structures and areas in order to ascertain high and low ends of alteration for nodules. For bivalves and cements, images were taken of bivalves, as well as the adjacent calcite cements. These images were taken on high powers to capture the crystalline detail, and cropped to eliminate sand grains in the field of view. Glue holes and slide edges were also cropped out of images.

4. RESULTS

Isotopic results are presented in Appendix 1 and were statistically analyzed via a combination of Minitab plots, Excel tests, MATLAB scripts, and tests done in StatsPlus Pro software. These results are presented in Appendix 2. Datasets from the Fossil Ridge site from Crystal (2014) and Foreman et al. (2015) were incorporated into this analysis, as well as data from Sicard (2004) from a site further away known as "The Blues" (V108/KS-20). Normality was tested using normal probability plots and Anderson-Darling tests on individual sets of samples from each site. Bivariate plots of carbon and oxygen isotope ratios were created to look for differences between sites. Minitab was used to check variances and normality of carbon and oxygen ratios for suites of samples. The confidence level for this analysis was set at $\alpha = .01$. While most sets of samples exhibited relatively normal distributions (Appendix 2), the variances between sets was highly variable (due to small sample sizes). As a result of this, t-tests assuming unequal variances were used to test the null hypotheses that the means of separate samples were the same, against the alternate hypotheses of difference. Results of these tests are summarized in Appendix 3.

4.1 Statistical results

A suite of tests was utilized to interpret and understand the data collected for this project. Means of populations of samples were tested for normality, and were tested against different populations of samples to investigate patterns of bimodality and variability between elements representing different aspects of the paleo-landscape. Some elements displayed differences for carbon and oxygen, while some were only significant for one or the other. Averages and standard deviations for each set of materials were

computed for this project (Table 2). The most relevant results from this these statistics are differences in carbon for dentine and enamel, distinct bimodality for oxygen in the gar scales, and differences in oxygen for the fluvial bivalves, ponded bivalves, and gar, hadrosaur elements, crocodiles and nodules.

	$\delta^{18}O$ Mean	$\delta^{18}O$ (1σ)	$\delta^{18}O$ Median	$\delta^{13}C$ Mean	$\delta^{13}C$ (1σ)	$\delta^{13}C$ Median
Gar Mode 2	-10.83	0.72	-10.5	-5.62	1.03	-5.51
Gar Mode 1	-8.97	1.27	-8.44	-6.20	1.05	-6.29
Hadrosaur Dentine	-8.28	0.59	-8.29	-5.00	2.90	-5.71
Hadrosaur Enamel	-8.20	0.64	-8.20	-7.50	1.23	-7.47
Pedogenic Carbonates	-7.74	0.56	-7.74	-9.31	1.07	-9.40
Crocodile Enamel	-7.79	0.74	-7.86	-8.19	1.44	-8.81
Micrites	-11.23	0.35	-11.40	-6.69	0.22	-6.65
Bivalves Pond (Foreman et al., 2015)	-9.47	1.68	-9.30	-5.77	2.10	-5.60
Bivalves Fluvial (Foreman et al., 2015)	-13.15	1.86	-12.9	-4.04	1.46	-4.70
Pedogenic Carbonates (Foreman et al., 2015) **SMOW	-8.06	0.54	8.00	-8.65	0.80	-8.70

Table 2: Statistical summary. Averages and standard deviations from base data (VDPB), with the exception of pedogenic carbonates from Foreman et al. (2015), which are presented in SMOW.

Dentine was tested against enamel and pedogenic carbonate for oxygen and carbon. These tests yielded no significance for dentine and enamel, but demonstrated significance for dentine and pedogenic carbonates. The three sites with gar in both populations (V108/KS-20, 4362 and 4370) were significantly different individually for oxygen isotope ratios between mode 1 gar and mode 2 gar, as well as in combination with data from 4445 and 4776 (both of which only display one mode). For tests between

gar enamel and hadrosaur enamel, significant difference for oxygen was found between 4445, 4362, V108/KS-20 and 4776. Samples 4445 and V108/KS-20 were not significant alone, while 4776 and 4362 demonstrated significances individually. Hadrosaur enamel from 4418, 4362 and 4776 appeared be different from the enamel from V108/KS-20 and 4445. Samples V108/KS-20 and 4445 were from sandier sites, which had fewer aquatic microfossils. These samples were not significantly different for oxygen. Tests were also run between data from the Foreman et al., (2015) and EKP datasets. The Foreman et al. (2015) dataset sampled vertically up section, and included nodules and bivalves from above and below the 450m area. The Foreman et al. (2015) nodules and the nodules from this dataset were not different for oxygen or carbon. However, when plotted in a bivariate scatter plot, Foreman et al. (2015) nodules appear to have higher values than those in this dataset, although there is some overlap between the two.

Foreman et al. (2015) bivalves had a larger range of stratigraphic heights. These bivalves were statistically significant for oxygen from the gar collected for this study. Fluvial bivalves displayed higher oxygen isotope ratio when compared to ponded bivalves. Additionally, there are the two populations of bivalves closest to the sampling elevation for this thesis (heights 325/365 and 445/315). Heights 325 and 365 fall into gar mode 2, while 445 and 315 fall into mode 1. The tests that are the most valid for these are those that test one material against itself, rather than against a different material (e.g. gar vs bivalves). This is because different animals impart a variable temperature fractionation when forming apatite, ganoine, or calcite. Temperature correction calculations only estimate temperature, and cannot account for inter-annual and annual variations in temperature.

Dentine data were significantly different from enamel for carbon. Similarly, pedogenic carbonate and dentine displayed significant differences for carbon. Enamel and pedogenic carbonate were different for carbon as well, both lumped together and individually. Carbon mean isotopic differences for all samples of gar were not significant. Individual sites were not significant with the exception of 4362. For nodules against enamel, lumped tests yielded significance. Samples from 4418 were not significant for differences in mean carbon between the two materials, while 4445, 4776 and V108/KS-20 were statistically significant. Gar enamel and hadrosaur enamel also showed difference for carbon with lumped samples, while 4445 and 4776 alone were not significant, and 4362 and V108/KS-20 demonstrated significant differences. A T test for difference in means for carbon between the Foreman et al. (2015) and the gar and bivalves from this dataset did not yield statistically significant differences. Carbon in hadrosaur enamel for 4418, 4362, 4776 against V108/KS-20 and 4445 did show a statistical difference. Additionally, micrite material from 4362 and 4445 was significantly different for both oxygen and carbon when tested against nodules.

4.2 Results from clumped isotope thermometry

Clumped isotope temperatures estimated for the suite of nodules are presented in Appendix 4. Calculated degrees of alteration for various areas of nodules and cements are presented in Appendix 5. In general, the centers of nodules appeared to be the least altered zones. Rims and edges were highly variable between samples, however they tended to display greater alteration. Vugs and veins also displayed higher alteration than pure centers, however these elements tended to be a relatively minor part of the nodule surfaces. Images taken of the whole nodules were cropped in Adobe Photoshop, and were

then used to calculate 'whole rock alteration %', which was used as the most representative degree of alteration for sites. Sites 4370 and 4418 have the lowest whole rock alteration indexes, as well as less alteration in the centers. Both of these nodules sets contain significant secondary growth in the form of veins and crystalline vugs. Averages for these calculations are presented in Table 3.

Sample #	Temperature	Whole Rock Alteration %	Center	Edge	Vug/Vein	Bivalve	Cement
4370 N3	53	20.47	15.47	30.33	15.62		
4370 N2	41	32.26	25.83	37.38	15.17		
4418 N1	53	33.73	27.01	33.31	48.00		
4418 N3	44	40.17	26.73	53.60	N/A		
4445 N2	48	45.658	38.89	50.34	N/A		
4445 N3	41	45.38	45.53	44.90	N/A		
4776 N1	47	34.91	31.93	N/A	36.41		
4776 N2	52	55.31	33.87	89.85	N/A		
Bivalve Site	58	56.79	N/A	N/A	N/A	56.80	39.67
CDM Site	72	40.79	N/A	N/A	N/A	44.39	40.49

Table 3: Clumped isotope temperatures and alteration percent.

5.DISCUSSION

5.1 Preservation of primary isotopic information

In order to study Cretaceous hydrology, it is necessary to demonstrate that primary isotopic information is preserved. There are two ways of doing so: 1) isotopic comparison of dentine and enamel from the same element, and 2) isotopic comparison of different species from the same site. Dentine is much more subject to alteration than enamel, and therefore the carbon isotope ratio in dentine should be significantly different than that of the enamel. This is verified up by T-tests for carbon between dentine and enamel on the same element (Appendix 2). Plots of enamel and dentine also show high and physiologically unreasonable $\delta^{13}C$ values in dentine relative to enamel, which is indicative of soil processes altering the carbon isotope ratios, and is consistent with findings from Crystal (2014). Comparisons between different species inhabiting the same location should yield isotopic offsets, as animals utilize carbon and oxygen differently through their metabolic pathways (Fricke et al., 2008). This is demonstrated in Figures 6 and 7, which highlight the difference between ganoine, crocodile and hadrosaur enamel from the same sites. Additionally, t-tests of enamel yield statistically significant results indicating difference between the taxa.

5.2 Using carbonate proxies to infer $\delta^{18}O$ of ancient water

In order to use $\delta^{18}O$ of bivalve shell aragonite, vertebrate tooth enamel, and body scales of fish to infer $\delta^{18}O$ of water these animals ingested, it is necessary to account for isotopic fractionations that take place when these materials form. In the case of bivalve shell aragonite, the empirical correlation derived by Kohn and Dettman (2007) is used to infer $\delta^{18}O$ of river and pond water (Table 4). This regression is robust for MAT >10°C, which can safely be assumed for the Kaiparowits based on flora (Wolfe and Upchurch,

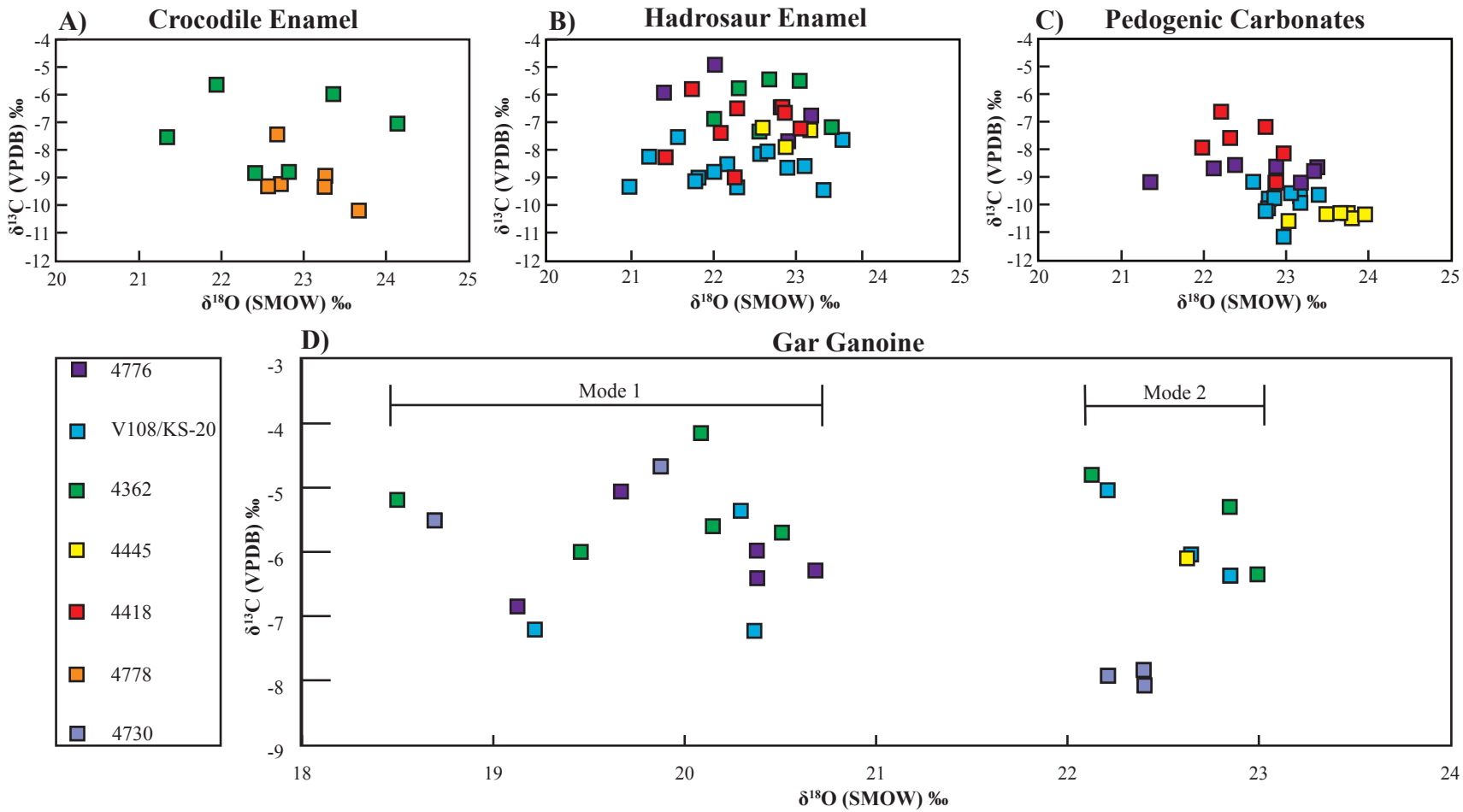

Figure 6: **Plot of data in SMOW calcite.** Top: Crocodile enamel, hadrosaur enamel, and pedogenic carbonates (soil nodules) from 4776, V108/KS-20, 4362, 4445, 4778 and 4418. Values have been translated into SMOW of calcite, not water. Bottom: Gar ganoine from 4445, V108/KS-20, 4730, 4362 and 4776. Bimodality of gar data can be seen in the lower plot.

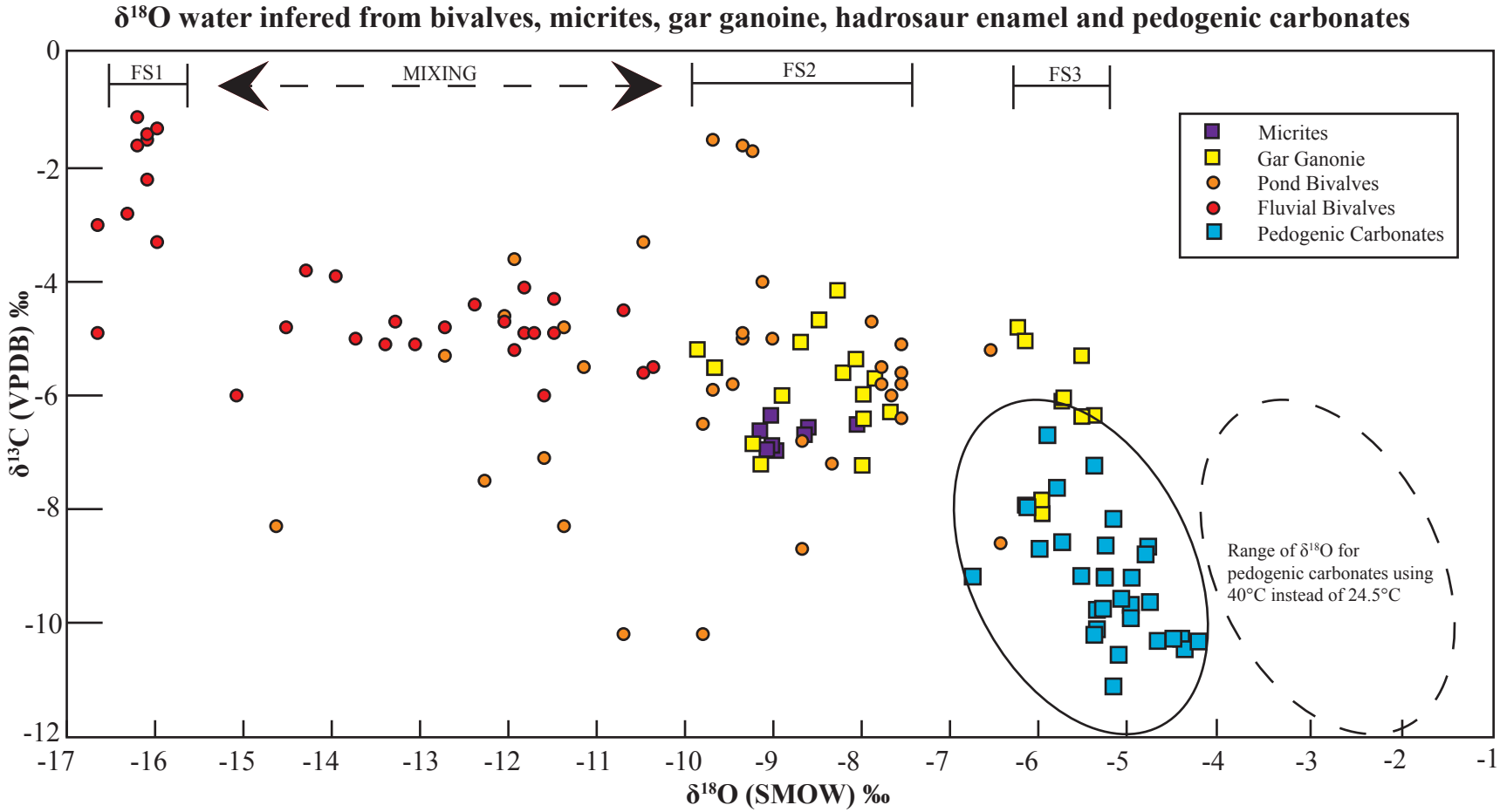

Figure 7: Plot of inferred water data. Values have been converted to water based on temperature fractionation (equations in Table 2). The three types of fluvial systems can be seen in the top of the plot. Mixing occurs between FS2 and FS1 as result of FS1 water backing up into the basin during monsoon season floods. Soil carbonates appear to be forming adjacent to locally sourced streams and rivers. Ovals indicate change in range for oxygen isotope ratios using 24.5°C (low end) and 40°C (high end) for temperature estimates.

1987; Miller, 2014). The empirically derived fractionation equation of Amiot et al. (2007), (corrected for application to carbonate) and the equations of Lecuyer et al. (2010) are used to infer the $\delta^{18}O$ of crocodile and gar ingested water, respectively. Lastly, a modified version of the physiological model developed by Kohn (1996) is used to infer the $\delta^{18}O$ of hadrosaur drinking water, again correcting for use with carbonates and assuming homoeothermic dinosaurs were physiologically similar to large mammals. This equation uses a humidity value of 0.85 because this value is the average humidity for the Tonle Sap lake system in modern-day Cambodia that functions as an analog for the Kaiparowits fluvial systems in this thesis (Tsujimoto, 2002).

EQUATION	APPLICATION	SOURCE
$\delta^{18}O$ (SMOW)= 1.03091 * ($\delta^{18}O$ VDPB) + 30.91	Conversion of data in VDPB to SMOW	Coplen et al., (1983)
$\delta^{18}O_{shell}$ (VDPB) = 0.89 * $\delta^{18}O_{river\ water}$ (VSMOW) – 0.98	Conversion of bivalve calcite values (VDPB) to river water (SMOW)	Kohn and Dettman, (2007)
$\delta^{18}O_{water} = 0.82*\delta^{18}O_{apatite}$ -27.13	Conversion from crocodile apatite to SMOW water	Modified from Amiot et al., (2007)
1000 ln $\alpha(CO_3^{2-}—H_2O)$ = 25.19 (±0.53)*T^{-1} -56.47 (±1.81)	Conversion from gar apatite to water (SMOW)	Lecuyer et al., (2009)
$\delta 18O_{calcite}$- $\delta^{18}O_{water}$ = 1000*ln(α)= (2.87 * $10^6/T^2$) – 2.89 (T in K)	Conversion of calcite to water for pedogenic carbonates	Kim and O'Neil, (1997)
$\delta^{18}O_{water}$= ($\delta^{18}O_{calcite}$-34.8-8.9(h))/0.76	Conversion to river water for hadrosaur enamel	Modified from Kohn, (1996)

Table 4: List of equations for water conversion.

In the case of paleosols carbonate nodules, the calcite–water fractionation equations of Kim and O'Neil (1997) were used to infer $\delta^{18}O$ of soil water. Temperatures at which nodules form, however, are uncertain. MAT for the Kaiparowits has been estimated at 22° C based on fossil leaf assemblages found throughout the formation (Miller et al., 2013). Nodules are known to form during the driest parts of the year, which are typically the summer months (Breecker et al., 2009; Peters et al., 2012). Quade et al. (2007) suggests that modern soil temperatures are typically 2.5°C warmer than MAT, and based on this observation previous studies of Kaiparowits nodules have assumed a formation temperature of 24.5°C (e.g., Foreman et al., 2015). In their study of carbonate soil nodules associated with the greenhouse climate of the Eocene, Snell et al. (2014) suggests that nodules form 10-15°C higher than MAT, in which case the Kaiparowits nodules may have formed at temperatures closer to 40° C. It was hoped that clumped isotope temperatures produced from Kaiparowits nodules (Table 4) would eliminate the need to assume formation temperatures, but the majority of the calculated estimates appear to be unrealistically high. Nevertheless, the lowest clumped isotope temperature estimates of ~ 40°C are close to those observed in other hothouse climates (Snell et al., 2013), and may represent unaltered values. However, only a few nodules averaged this temperature, and there was enough evidence for diagenic alteration in the nodules sampled to require more sampling before using the 40°C temperature. Therefore a temperature of 24.5°C was used to estimate $\delta^{18}O$ of soil water temperature (Figure 7), keeping in mind temperatures may have been higher and thus estimated $\delta^{18}O$ soil water could be higher (Figure 7, dashed shape).

Because oxygen undergoes a temperature dependent fractionation, differences in populations and ranges were more important for animal, bivalve and paleosol data than absolute oxygen isotope ratios. The temperature effect of fractionation during formation of nodules and biologic hard part precipitation need to be taken into account when providing a complete analysis. Relative differences between populations of the same material should be close for VDPB and SMOW standards. Equations used to convert data into SMOW and from calcite to water can be found in Table 4. Additionally, data are also presented in ‰SMOW values, uncorrected for water, which display the same patterns as plots for water (Figure 6). Data display the same patterns and have statistical differences still exist after these estimates are made.

5.3 δ^{18}O of ancient waters and hydrology at the catchment scale

5.3.1 Characterizing bodies of water occupying a landscape

A plot of δ^{13}C carbonate versus estimated δ^{18}O water (Figure 7) along with considerations of sedimentological context can be used as a basis for making interpretations regarding hydrological patterns in the Kaiparowits basin at the catchment scale during the Late Cretaceous (Figure 8). Based on the distribution of different lithologies in conjunction with $\delta^{18}O_{sf}$, and variability in the types of aquatic animals (e.g. bivalves, gar fish, crocodiles), there appear to be three distinct types of water bodies present over the landscape. The first is termed fluvial system 1 (FS1), and it is characterized by low δ^{18}O averaging -16‰ and lower. This fluvial system is represented by bivalves from large sandstone channels. δ^{18}O from these bivalves is statistically different from the bond bivalves and from gar.

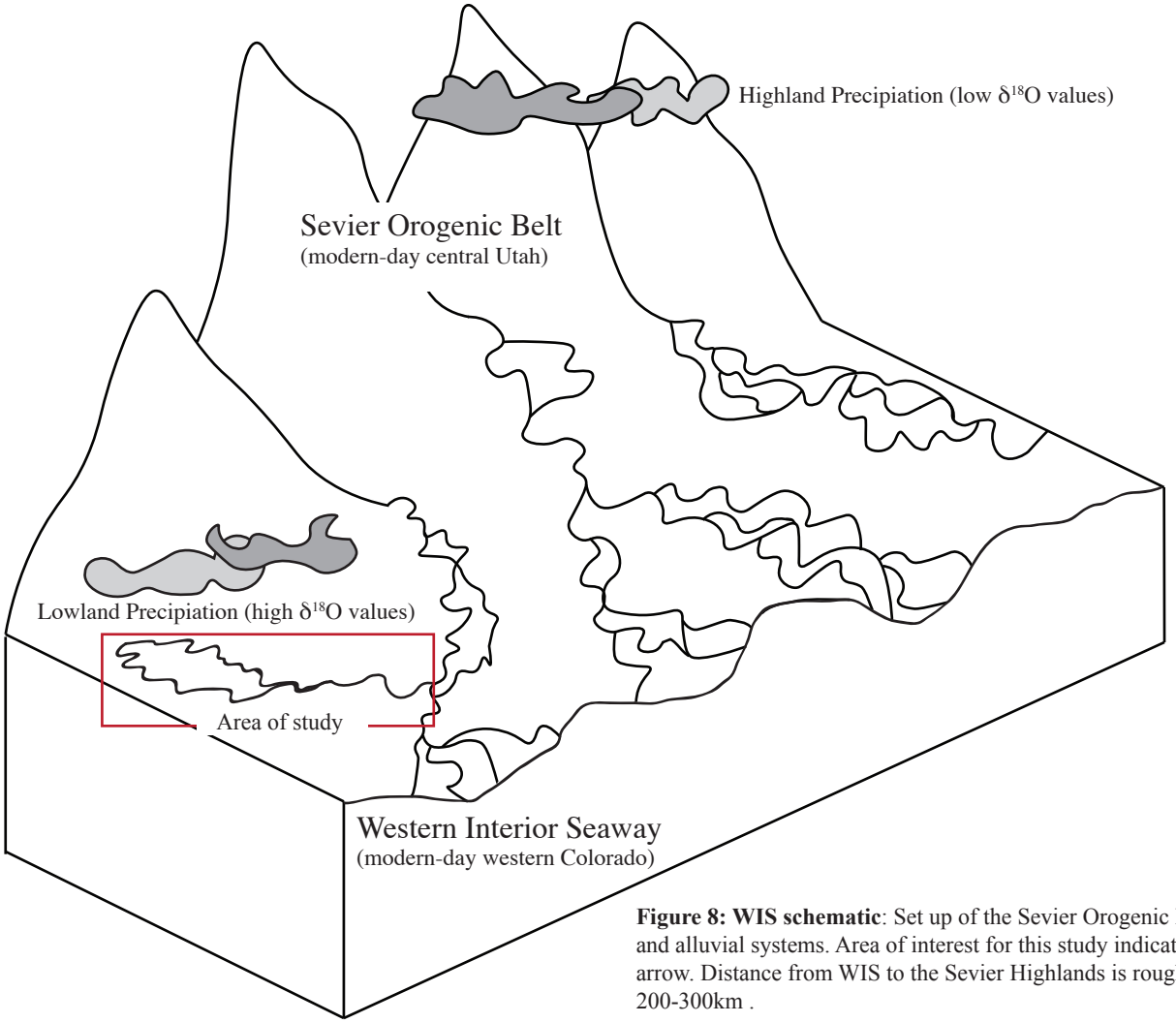

Figure 8: WIS schematic: Set up of the Sevier Orogenic Belt, WIS and alluvial systems. Area of interest for this study indicated by red arrow. Distance from WIS to the Sevier Highlands is roughly 200-300km .

The second fluvial system is termed FS2 and is characterized by $\delta^{18}O_{sf}$ of -9‰. This system is shown in Figure 9, and is represented by ponded bivalves and gar having the lowest $\delta^{18}O_{sf}$ (gar mode 1, Figure 6). Micrite data also overlap with this fluvial system. This system as a whole is statistically significant from FS1, and is characterized by organic rich mudstones and siltstones interpreted to be overbank ponds and paleosols. The sites associated with FS2 contain a more lacustrine lithology, including fine muds and silts, as well as predominance of aquatic animals (gar fish, crocodiles, and turtles). Lastly, there is a third component, FS3, characterized by a higher $\delta^{18}O_{sf}$ of -6‰. This system is represented by the mode 2 gar (Figure 6). The gar found in FS3 are mode 2 gar, and have higher $\delta^{18}O$ values, and do not overlap with the bivalve data.

The relationship of soil water inferred from pedogenic soil carbonate nodules is uncertain. If the high temperatures of formation are correct, then these nodules appear to form in soils hydrologically disconnected from the lake and stream systems. If the low temperatures of formation are correct, then these materials appear to be forming in association with FS3 streams and rivers. For paleosol carbonate, higher temperatures generally correlate with higher degrees of alteration. The least altered nodules were from 4418 and 4730. However, these values did not correlate to lower temperatures, and upon further inspection sampling sites seem to be closer to vugs and veins. Therefore, the sites that have the least alteration for the centers, unaltered sample sites and correspondingly low temperatures appear to be the closest approximations to soil temperature for this dataset. The lowest clumped isotope temperature is to 16°C higher than estimates based on paleo flora. While this value is not out of the question, further work needs to be done to validate these soil temperatures. As a result, corrections for SMOW for nodules were

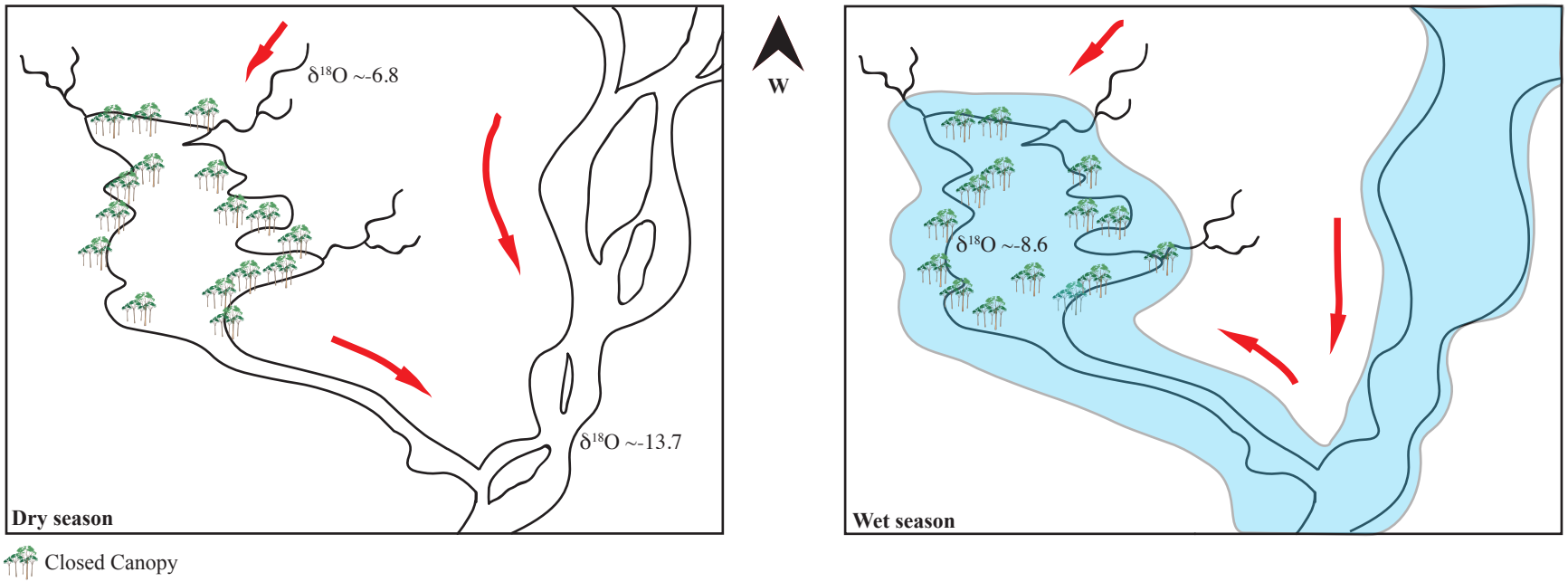

Figure 9: Flooding of the Kaiparowits landscape. Left: dry season, rivers flowing to WIS. Large anastomosing river systems meet with rivers flowing out of the basin. These large rivers are sourced in the highlands, and have relatively high $\delta^{18}O$ values (~16-18‰). Perennial standing water/small lakes fill lowland areas in the basin and are fed by local precipitation giving smaller streams and waterways relatively $\delta^{18}O$ values (on average ~3‰). Ponded standing water in the basin displays a mixing signal as a result of highland water backing up into the basin during the wet season (right panel) and flooding the landscape. Carbon-rich sites would have been located more proximally to the basin low, while drier and sandier sites would have been found on the interfluves. Sites closer to standing water would have been under a thick canopy, while the floodplain and source streams would have been under a much less dense canopy with oxidation occuring in the soils. Changes in flow direction indicated by red arrows.

calculated using both the Miller (2014) MAT + 2.5°C, not the 41°C determined by this line of investigation.

5.3.2 Hydrological interpretations

It is possible to reconstruct the movement of water over the Kaiparowits landscape. FS1 would have contained waters derived from high elevations, as evidenced by the low $\delta^{18}O$ of water is indicative of water sourced in systems where ^{18}O has been precipitated out of the system as water moves across land. Additionally, deposits associated with FS1 systems are dominated by sand, indicating a higher energy fluvial environment with a more distal source. FS2 contains a mixture of highland and lowland waters, as indicated by the intermediate $\delta^{18}O$ values. This freshwater standing lake would have experienced mixing during flooding season. Lastly, FS3 water has the highest oxygen isotope ratios, indicating that this water was sourced from precipitation falling over the coastal lowlands, recharging small streams and ponds standing on the floodplain. Water was sourced locally before elevation-driven fractionation could have removed the heavier isotope of oxygen from rainout.

5.3.3 Relating waters on the landscape, and the Tonle Sap analog

Taking all of these interpretations together, and considering a modern analog system, it is possible to develop a model of what Kaiparowits basin floodplains may have looked like during the Late Cretaceous, and how the FS1, FS2 and FS3 systems related to each other hydrologically. Figure 8 shows the assumed position of this sub basin on the floodplain adjacent to the WIS. The FS1 rivers are inferred to have flowed from the highlands out to the coast. Smaller local rivers and streams (FS3) are inferred to have been fed by local meteoric precipitation. The lake system is inferred to have been

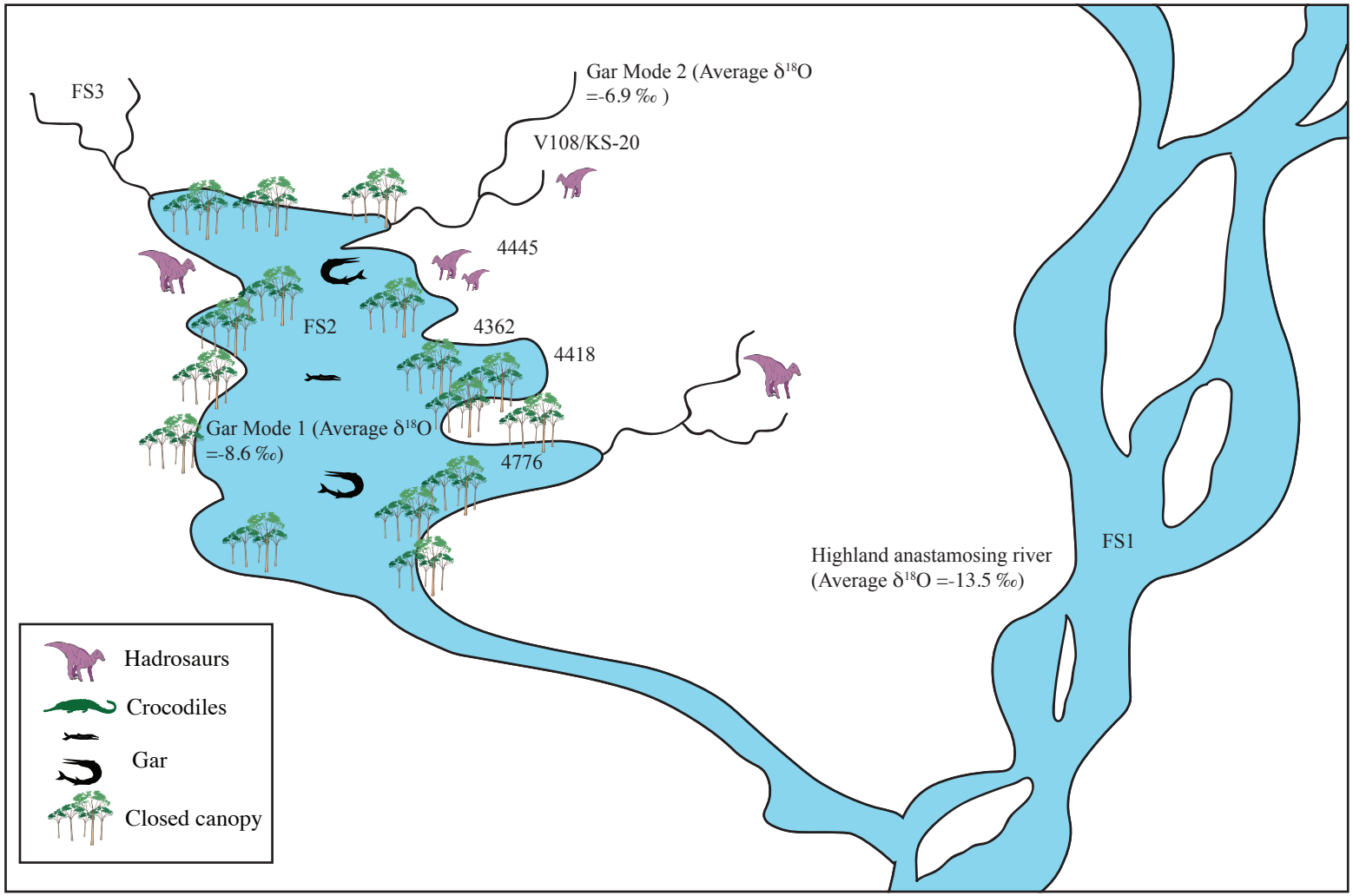

Figure 10: Relative location of sites incorporated into this study on the floodplain. Sites missing from this image are lacking in complete suites of these materials. The nature of vegetation around FS1 cannot be inferred from this dataset, however water values are known from Foreman et al, 2015. 4776 contains only Mode 1 gar, which indicates it was possibly closer to the lake. This site also contains an abundance of crocodiles, fish and turtles, indicating it was aquatic. 4362 contains lacustrine carbonates, which indicates it was deposited in a marginal lake setting. 4418 appears to be less aquatic and less canopied, indicating it was farther out on the floodplain. 4445 and V108/KS-20 appear to have been the most open, and would then be located on the interfluves farther away on the floodplain.

connected to the other two, as evidenced by micrites and adjacent nodules indicating evaporation and drying.

This interpretation presents a paradox: the lake should have $\delta^{18}O$ similar to the streams feeling into it, or possibly higher $\delta^{18}O$ due to evaporation, but the $\delta^{18}O$ is lower. To explain this paradox, it is suggested that during the monsoon season the rivers would have backed up into the lake, increasing lake levels and resulting in 1) mixing of FS1 and FS3 water and 2) deposition of material on the aprons of small streams feeding into the lake. Figure 9 illustrates the backing up of water into the lake during the wet season, and the reversal in flow directions that would have occurred as a result. The ponded marsh in the middle of the basin would have been recharged by both local streams and water coming in from the anastomosing river systems sourced in the highlands. This gives the mixing signature seen in the lake gar (gar mode 1) and the micrites and soil nodules found along the margins of the perennial water body. This area would have been fed primarily by small rivers and streams during the dry season.

The closest modern analog to this type of hydrologic landscape is the Tonle Sap Lake in central Cambodia. This lake is peripheral to the Mekong River Basin which originates in the Tibetan Highlands. This catchment is defined by the anastomosing Mekong River which flows to the South China Sea at the Mekong River Delta. Tonle Sap Lake is located ~350 km upstream, and to the west of this delta. This lake has highly variable volume, and experiences flow reversals as a result of flooding during the monsoon season. During the monsoon season, the Mekong River backs up into the Tonle Sap River, which increases the flow into the lake and volume of the lake dramatically, inundating adjacent wetlands (Kabeya et al., 2008). At the end of the monsoon season,

water level falls, and flow direction of the draining channel reverses. In fact, The Tonle Sap River flows in opposing directions for 50% of the year. This reversal in flow direction occurs as the result of the highly constrained nature of the Mekong River, as well as the topographic highs to north and south, which constrain flow and prevent it from flowing out to the sea. The Tibetan Plateau is similar in elevation to elevations presumed for the Sevier Orogenic Belt (Sewall & Fricke, 2013; Foreman et al., 2015), and the relatively flat slope of the Kaiparowits is similar in relief to modern-day central Cambodia.

This model provides for the possibility of perennial ponded water with formation of micrite and nodules on the margins, and an adjacent floodplain fed by smaller rivers and streams that was inundated during the wettest months of the year. If this model serves for the Kaiparowits sections of interest, it is reasonable the mixing line between the lowest gar populations, micrite and ponded and fluvial bivalves. If water was backing up into a basin adjacent to a large river sourced in the highlands, this scenario could account for the zone of mixing, and distinct modes of gar (Kabeya et al., 2008).

5.4 Variation in soil drainage, forest structure and dinosaur behavior associated with lake margin systems

5.4.1 Oxidation state of soils and location along the lake margin

If the above interpretations are correct, then the mud/silt paleosols sampled as a part of this study were located along the margins of the lake with seasonally variable shorelines. Percent TOC and fossils can be used to suggest their relative position with respect to the center of the lake. The differences between sites in terms of soil color; %TOC, and distribution of vertebrate fossil material may be an indication as to the state

of oxidation and drainage state of soils. Better drained soils were positioned farther away from the lake, while less oxidized darker soils would have been located along the lake margins. The oxidation state of these soils is also an indicator for forest structure over the landscape. With this in mind, 4362 would have been close to the lake margin, V108 and 4445 would have been far away with the other sites in between (Figure 10). Site 4362 is a dark mudstone site, with high %TOC, no nodules and a diversity and abundance of fossils. This site contains whole gastropods, and is found adjacent to nodule and micrite beds. The high %TOC and high $\delta^{13}C$ values indicate that this site was poorly drained, poorly oxidized. Percent TOC is higher when there is less oxidation occurring in soils. Similarly, high $\delta^{13}C$ ratios are indicative of methane processes which occur in poorly drained soils. On the opposite end of the spectrum, 4445 and V108/KS-20 are sandier, contain fewer carbon and charcoal blebs indicating they were likely drier for more of the year. These sites also host carbonate nodules which require soils experience aridity for some of the year (Cerling and Quade, 1993). This would have been most likely during the dry season of the monsoon and would have dried out during the rest of the year to form paleosols

5.4.2 Canopy structure

The other question that arises with this dataset is the nature of the canopy over these wetland landscapes. Crystal (2014) used enamel and dentine from dinosaur fossils from microsites located within the ~450m section range, and analyzed simple bulk isotopic compositions. This work indicates that there are significant statistically differences in $\delta^{13}C$ ratios between sites (see Figure 6, panel B). This offset could be the result of behavior differences between animals (i.e. niche partitioning), or the result of

differences in microenvironments across the landscape (closed vs. open canopy). The most viable explanation for this difference is the canopy effect. CO_2 would have been recycled in the understory of a closed canopy system, therein modifying the $\delta^{13}C$ values found in understory plants, which would have, in turn, been consumed by the dinosaurs giving them an isotopically distinct signature. A closed canopy system keeps carbon on the understory, and reduce the possibly of mixing with atmospheric carbon. This results in more negative $\delta^{13}C$ values, as plant carbon is recycled through the carbon cycle with less input from more positive carbon source. Closed canopies also alter the photosynthetic processes and availability of light and oxygen in the understory (Crystal, 2014; Drucker et al., 2008).

The data presented in this thesis provide more evidence (through dentine isotopic ratios) for a closed canopy on the floodplain of the Kaiparowits. Equally important lithological contrasts are described above and also support variations in canopy structure. Based on the relative ratios of carbon isotopes in hadrosaur enamel from these sites, it appears that they experienced more of an open canopy than 4362, 4776 or 4418. Sites 4362, 4776 and 4418 display higher $\delta^{13}C$ values, which is an indicator for methane production in soils. This relationship means the lake margins would have been covered by a closed canopy. The opposite end of the spectrum would have been V108/KS-20 and 4445, drier sites, likely located further from the lake margin, vegetated but not covered by a closed canopy. These sites would have been covered during monsoon season floods, but dry during the rest of the year. The $\delta^{13}C$ ratios expressed in dentine and enamel for these sites also support this conclusion. The relative ratios of $\delta^{13}C$ in the 4362, 4776 and 4418 sites are statistically different from the enamel of the same tooth (because they have

undergone diagenesis) but are also statistically different from V108/KS-20 and 4445 sites in terms of carbon.

5.4.3 Dinosaur behavior

The $\delta^{18}O$ ratios present in the hadrosaurs used in this study plot under the mode 1 gar. This gar reflects the mixing of highland rivers and local streams in ponded waters. Hadrosaur data falls between FS1 and FS2 which means that these animals were likely drinking from both sources of water, as would be expected of a mobile animal. Pedogenic carbonate shown in the same plot fall underneath the mode 2 gar, which indicates that these carbonate were forming in waters with higher $\delta^{18}O$ values, farther away from the central low of the basin, although there is uncertainty with the estimates for temperature with those values. Evaporation fractionates against ^{16}O, which results in ponded water $\delta^{18}O$ values higher than those of the water that feeds into a ponded area (Talbot, 1990). In arid settings, $\delta^{13}C$ and $\delta^{18}O$ tend to display a positive covariance as a result of progressive evaporation. The pedogenic carbonate in this study displays a negative covariance, which provides further support for methane production, and indicates that this environment was extremely humid with very little evaporation of water off the floodplain.

6. CONCLUSION

This dataset provides interesting and previously unexplored insights into the hydrologic systems of the Late Cretaceous, specifically systems in transition as a result of uplift. The bimodality of the ganonie data, in conjunction with the mixing line seen in bivalve data provides convincing evidence for restriction of fluvial systems to limited basin, with climate driven monsoon precipitation moving waters between basins and rivers for a limited period of time. Additionally, carbonates, hadrosaurs, and micrite can be positioned on the floodplain as a result of their isotopic ratios. The bimodality of the gar ganonie is interesting from an ecological standpoint, because if animals were moving back and forth between locations one might expect to see a mixing line in the data obtained from scales. Instead, two distinct modes are present, one with relatively high $\delta^{18}O$ values, and one with low $\delta^{18}O$ values. The low value mode falls along the high end of the ponded bivalve data (Foreman et al., 2015), which is statistically distinct from the fluvial bivalves sampled in the same study. The bimodality of the ganonie data indicates that these animals were biologically restricted, and likely inhabited distinct niches. Flooding would have moved gar across the landscape and deposited them on the apron adjacent to ponded lake water in the center of the basin during the monsoon season. Water would have then retreated into the dry season, and gar would have returned to their respective environments of preference. Sites with different lithologies contain both modes of gar (V108/KS-20, 4362 and 4730), while two sites only exhibit one mode (4445 and 4776). Site 4445 does not have enough data to be statistically significant, although site 4776 has five discrete data points. The distinct separate modes of gar ganonie indicates that these animals were imparted with their isotopic signatures during their life spans, and then died in their final

resting sites shortly after flooding events. Hadrosaurs were not likely to be restricted to a specific environment, and display a signal of mixing between the FS1 and FS2 systems. Pedogenic carbonate appears to have formed on the interfluves of local streams and rivers, while micrites form adjacent to ponded water in the low centers of the basin.

An additional component of this project is the refinement of the nature of the canopy proposed in Crystal (2014). The inundated basin lowlands were covered by a closed canopy, which resulted in reduced oxidation and increased methane production in soils. The higher edges of the basin were more open, and experienced a greater fluctuation in soil inundation and aridity. The analog of the modern Tonle Sap lake provides an additional line of evidence for this system. The adjacent limited river systems, low lying flood plain, and highland topography are analogous to Late Cretaceous systems. Future projects could potentially investigate the nature of wetland isotope ratios in relations to the Mekong River and lake itself. Isotopic ratios in modern fish found in this system could also provide for an interesting project to validate the interpretations put forward in this thesis.

WORKS CITED

Amiot, R., LeCuyer, C., Escarguel, G., Billon-Bruyat, J.-P., Buffetau, E., Langlois, C.,Martin, S., Martineau, F., And Mazin, J.M., 2007. Oxygen isotope fractionation between crocodilian phosphate and water: Palaeogeography, Palaeoclimatology, Palaeoecology, 243 (412–420).

Ball, J., 2016, Reconstructing forest structure in southern Utah during the late Cretaceous, Unpublished Thesis.

Beerling, D., Berner, R.A., Mackenzie, F. T., Hartfoot, M.B., Pyle, J.A., 2009, Methane and the CH_4 – related feedbacks in past greenhouse worlds. PNAS 108, 24 (9770-9775).

Blakey, R. Late Cretaceous, 75 my. Colorado Plateau Geosystems.

Breecker, D.O., Sharp, Z.D., McFadden, L.D., 2009, Seasonal bias in the formation and stable isotopic composition of pedogenic carbonate in modern soils from central New Mexico, USA. Geol. Soc. Am. Bull. 121, 630–640.

Cerling, T. E., 1984, The stable isotopic composition of modern soil carbonate and its relationship to climate. Earth and Planetary Science Letters. 71.

Celing, T.E., Quade, J., 1993, Stable carbon and oxygen isotopes in soil carbonates. Climate Change in Continental Isotopic Records. American Geophysical Union.

Chivas, A. R., Dux, F. W., 2015, Clumped isotope geochemistry. Principles and practice of analytical techniques in geosciences. Royal Society of Chemistry.

Crystal, V. F., 2014, Variations in Hadrosaurid behavior, soil processes, and forest structure over the Late Cretaceous landscape of southern Utah (Kaiparowits Formation, Grand Staircase Escalante National Monument). (Unpublished senior thesis).

Coplen, T.B., Kendall, C., And Hopple, J., 1983, Comparison of stable isotope reference samples: Nature, 302, (236–238)

DeCelles, P. G., Giles, K. A., 1996, Foreland Basin Systems. Basin Research (8).

Dennis, K.J., Affek. H.P., Passey, B.H., Schrag, D.P., Eiler, J.M., 2011, Defining and absolute reference frame for 'clumped isotope' studies of CO_2. Geochimica et Cosmochimic. (75).

Dettman, D. L., Reische, A.K, Lohman K.C., 1998, Controls on the stable isotope composition of seasonal growth bands in aragonitic fresh-water bivalves (unionidae). Geochimica et Cosmochimica Acta 63 (7/8).

Drucker, D. G., Bridault, A., Hobson, K. A., Szuma, E., and Bocherens, H., 2008,

Can carbon-13 in large herbivores reflect the canopy effect in temperate and boreal ecosystems? Evidence from modern and ancient ungulates: Palaeogeography, Palaeoclimatology, Palaeoecology. 266 (69-82).

Eiler. J. M., 2007, Clumped-isotope_ geochemistry-the study of naturally-occurring, multiply-substituted isotopolouges. Earth and Planetary Science Letters (262).

Evans, D. C., Williamson, T., Loewen, M. A., Kirkland, J. I., 2013, A Review of Pachycephalosaurian dinosaurs from Grand Staircase-Escalante National Monument, southern Utah. *At the top of the Grand Staircase, the Late Cretaceous of Southern Utah.* Ed. Titus, A. L., Loewen, M. A. Bloomington Indiana, Indiana University press, 2013. Print

Foreman, B.Z., Roberts, E. M., Tapanila, L., Ratigan, D., Sullivan, P., 2015, Stable isotopic insights into paleoclimatic conditions and alluvial depositional processes in the Kaiparowits Formation (Campanian, south-central Utah, U.S.A.). Cretaceous Research (56).

Foreman, B.Z., Fricke, H. C., K.C. Lohmann, Rogers, R.R, 2011, Reconstructing paleocatchments by integrating stable isotope records, sedimentology, and taphonomy: A late Cretaceous case study (Montana, United States). PALIOS, 26 (545-554).

Fricke, C.H, Raymond, R.R., Gates, T.A., 2009, Hadrosaurid migration: inferences based on stable isotope comparisons among Late Cretaceous dinosaur localities, Paleobiology 35 (2).

Fricke, H. C., Pearson, D. A., 2008, Stable isotope evidence for changes in dietary niche partitioning among hadrosaurian and ceratopsian dinosaurs of the Hell Creek Formation, North Dakota. Paleobiology. 34 (4).

Fricke, H. C., Foreman, B. Z., Sewall, J. O., 2010, Integrated climate model-oxygen isotope evidence for a North American monsoon during the Late Cretaceous. Earth & Planetary Science Letters (289).

Fricke, H.C., Roger, R. R., Backlund, R., Dwyer, C.N., Echt, S., 2008, Preservation of primary stable isotope signals in dinosaur remains, and environmental gradients of late Cretaceous Montana and Alberta. Palaeogeography, Palaeoclimatology, Palaeoecology. 266.

Fricke, H. C., 2007, Stable isotope geochemistry of bonebed fossils: reconstructing paleoenvironments, paleoecology, and paleobiology. Rogers, R. R., Eberth, D. A., Fiorillo, A. R., (eds). Bonebeds, genesis, analysis and paleobiological significance. University of Chicago Press.

Gates, T. A., Lund, E. K., Boyd, C. A., DeBlieux, D. D., Titus, A., Evans, D. C., Getty,

M. A., Kirkland, J. I., Eaton, J. G., 2013, Ornithopod dinosaurs from the Grand Staircase-Escalante National Monument Region, Utah, and their role in paleobiogeographic and macroevoloutionary studies. *At the top of the Grand Staircase, the Late Cretaceous of Southern Utah.* Ed. Titus, A. L., Loewen, M. A. Bloomington Indiana, Indiana University Press.

Huntington, K.W, Eiler, J.M, Affek, H.P, Guo, W., Bonifacie, M., Yeung, L.Y., Thiagarajan, N., Passey, B., Tripati, A., Daerson, M., Came, R., 2009, Methods and limitation of 'clumped' CO_2 isotope ($\Delta 47$) analysis by gas-source isotope ratio mass spectrometry. Journal of Mass Spectrometry. (44).

Irmis, R. B., Hutchinson, J. H., Sertich, J. W., Titus, A. L., 2013, Crocodyliforms from the late Cretaceous of the Grand Staircase-Escalante National Monument and vicinity, Southern Utah, U.S.A. *At the top of the Grand Staircase, the Late Cretaceous of Southern Utah.* Ed. Titus, A. L., Loewen, M. A. Bloomington Indiana, Indiana University press, 2013. Print.

Jahren, A. H., LePage, B. A., and Werts, S. P., 2004, Methanogenesis in Eocene Arctic soils inferred from δ13C of tree fossil carbonates: Palaeogeography, Palaeoclimatology, Palaeoecology. 214 (347-358)

Kabeya, N., Kubota, T., Shimizu, A., Nobuhrio, T., Tsuboyama, Y., Chann, S., Tith, N., 2008, Isotopic investigation of river water mixing around the confluence of the Tonle Sap and Mekong rivers. Hydrological Processes. 22 (1351-1358).

Kim, S.T., and O'Neil, 1997, Equilibrium and nonequilibrium oxygen isotope effects in synthetic carbonates. Geochimica et Cosmochimica Acta. 61(16).

Kluge, T., John, C.M., Jourdan, A.L., Davis, S., Crawshaw, J., 2015, Laboratory calibration of the calcium carbonate clumped isotope thermometer in the 25-50°C temperature range. Geochimica et Cosmochimica Acta. (157).

Koch, P. L., 1998, Isotopic reconstruction of past continental environments. Annual Review Earth and Planetary Sciences. 26 (573-613).

Kohn, M. J. and Cerling, T. E., 2002, Stable isotope compositions of biological apatite: Reviews in Mineralogy and Geochemistr*y*. 48 (1).

Kohn, M.J., And Dettman, D.L., 2007, Paleoaltimetry from stable isotope compositions of fossils: Reviews in Mineralogy and Geochemistry, v. 66, p. 119–154.

Kohn, M.J., 1996, Predicting animal $\delta^{18}O$ Accounting for diet and physiological adaptation. Geochimica et Cosmochimica Acta. 60 (23).

Le´cuyer, C., Balter, V., Martineau, F., Fourel F., Bernard A, Amiot R, Gardien V., Otero O., c, Legendre S., Panczer G., Simon L., Martini R., 2009, Oxygen isotope fractionation between apatite-bound carbonate and water determined from controlled experiments with synthetic apatites precipitated at 10–37°C. Geochemica et Cosmochimica Acta, 74 (2071-2081).

Loewen, M. A., Burns, M. E., Getty, M. A., Kirkland, J. I., Vickaryous, 2013, Review of Late Cretaceous ankylosaruan dinosaurs from the Grand Staircase Region, Southern Utah. *At the top of the Grand Staircase, the Late Cretaceous of Southern Utah.* Ed. Titus, A. L., Loewen, M. A. Bloomington Indiana, Indiana University press, 2013. Print.

Loewen, M., Farke, A., Sampson, S., Getty, M., Lund, E., O'Connor, P., 2013, Ceratopsid dinosaurs from the Grand Staircase of Southern Utah *At the top of the Grand Staircase, the Late Cretaceous of Southern Utah.* Ed. Titus, A. L., Loewen, M. A. Bloomington Indiana, Indiana University press, 2013. Print.

Miller, I., Johnson, K., Kline, D., Nicholas, D., Barclay. R., 2013, A late Campanian flora from the Kaiparowits formation, southern Utah, and a brief overview of the widely sampled but little-known Campanian vegetation of the Western Interior Seaway. *At the top of the Grand Staircase, the Late Cretaceous of Southern Utah.* Ed. Titus, A. L., Loewen, M. A. Bloomington Indiana, Indiana University press, 2013. Print.

Talbot, M.R., 1990, A review of paleohydrological interpretation of carbon and oxygen isotopic ratios in primary lacustrine carbonates. Chemical Geology (80).

Titus, A., Roberts, E., Albright B., 2013, Geologic Overview. *At the top of the Grand Staircase, the Late Cretaceous of Southern Utah.* Ed. Titus, A. L., Loewen, M. A. Bloomington Indiana, Indiana University press, 2013. Print.

Tsujimoto, K., 2002, Hydro-meteorological Environment at Tonle Sap Lake and its Environs: As a Case Study of Lake Basins in the Tropical Humid Region. National Institute of Rural Engineering (NIRE), Japan.

Peters, N.A., Huntington, K.W., Hoke, G.D., 2013, Hot or not? Impact of seasonally variable soil carbonate formation on paleotemperatue and O-isotope records from clumped isotope thermometry. Earth and Planetary Science Letters. (361).

Quade, J., Garzione, C., And Eiler, J., 2007, Paleo elevation reconstruction using pedogenic carbonates: Reviews in Mineralogy and Geochemistry, 66 (53–87).

Quade J., Breecker D.O., Daëron M., Eiler J., 2011, The paleoaltimetry of Tibet:An isotopic perspective: American Journal of Science, (311).

Roberts, E., Sampson, S., Alan, Deino, A., Bowring, S., Buchwaldt, R., 2013, The

Kaiparowits Formation: a remarkable record of Late Cretaceous terrestrial environments, ecosystems, and evolution in Western North America. *At the top of the Grand Staircase, the Late Cretaceous of Southern Utah.* Ed. Titus, A. L., Loewen, M. A. Bloomington Indiana, Indiana University press, 2013. Print.

Roberts, E. M., 2007, Facies architecture and depositional environments of the Upper Cretaceous Kaiparowits Formation of southern Utah. Sedimentary Geology. (197).

Sewall, J. O., Fricke, H.C., 2013, Andrean-scale highlands in the late Cretaceous Crodillera of the North American western margin. Earth and Planetary Science Letters. (362).

Sewall, J. O. and Sloan, L. C., 2006, Come a little bit closer: A high resolution climate study of the early Paleogene Laramide foreland, Geology, 34 (81–84).

Sicard, K., 2004, Unpublished research paper. Vertebrate excavation and isotopic analysis.

Whiticar, M. J., (1999), Carbon and hydrogen isotope systematic of bacterial formation andoxidation of methane. Chemical Geology, 161 (291-314).

Wolfe, J. A., Upchurch, G. R., 1987, North American nonmarine climates and vegetation during the Late Cretaceous. Palaeoegeography, paleoclimatology, paleoecology (61)

Zaaur, S., Affeck, H.P., Brandon, M.T., 2013, A revised calibration of the clumped isotope thermometer. Earth and Plantetary Science Letters. (382).

APPENDIX 1

Site	Sample ID	$\delta^{13}C$ VPDB	$\delta^{18}O$ VPDB	$\delta^{18}O$ SMOW	$\delta^{18}O$ (SMOW) WATER
4730	DMNS 4730 G4E	-5.51	-11.85	18.693	-8.307
4730	DMNS 4730 G5E	-8.08	-8.25	22.403	-4.597
4730	DMNS 4730 G1E	-7.93	-8.44	22.212	-4.788
4730	DMNS 4730 G6E	-7.84	-8.26	22.398	-4.602
4730	DMNS 4730 G3E	-4.67	-10.70	19.875	-7.125
4730	DMNS 4730 G4E	-5.51	-11.85	18.693	-8.307
4730	DMNS 4730 G5E	-8.08	-8.25	22.403	-4.597
4730	DMNS 4730 G1E	-7.93	-8.44	22.212	-4.788
4730	DMNS 4730 G6E	-7.84	-8.26	22.398	-4.602
4730	DMNS 4730 G3E	-4.67	-10.70	19.875	-7.125
4445	PH-G1E	-6.10	-8.04	22.625	-4.375
4362	4362-B G6E	-4.80	-8.52	22.127	-4.873
4362	# 72129 4362 G1E	-5.60	-10.44	20.147	-6.853
4362	# 72128 4362 G2E	-5.70	-10.09	20.508	-6.492
4362	4362-B G4E	-5.30	-7.82	22.848	-4.152
4362	4362-B G7E	-5.19	-12.04	18.498	-8.502
4362	# 72131 4362-B G3E	-6.35	-7.68	22.993	-4.007
4362	4362-A G8E	-6.00	-11.11	19.457	-7.543
4362	4362-B G5E	-4.15	-10.50	20.085	-6.915
4776	4776 G5E	-5.98	-10.22	20.377	-6.623
4776	4776 G4E	-6.41	-10.21	20.379	-6.621
4776	4776 G1E	-6.85	-11.43	19.126	-7.874
4776	4776 G2E	-6.29	-9.92	20.683	-6.317
4776	4776 G3E	-5.06	-10.91	19.667	-7.333
V108/KS-20	KS-20 G1E	-6.04	-8.02	22.646	-4.354
V108/KS-20	KS-20 G2E	-5.04	-8.44	22.210	-4.790
V108/KS-20	KS-20 G3E	-5.36	-10.30	20.293	-6.707
V108/KS-20	KS-20 G4E	-6.37	-7.82	22.851	-4.149
V108/KS-20	KS-20 G5E	-7.21	-11.34	19.217	-7.783
V108/KS-20	KS-20 G6E	-7.23	-10.23	20.364	-6.636
V108/KS-20	KS-20 G4E	-6.37	-7.82	22.851	-4.149

Data for gar ganonie from sites 4730, 4445, 4362, 4776 and V108/KS-20

Site	Sample ID	$\delta^{13}C$ VPDB	$\delta^{18}O$ VPDB	$\delta^{18}O$ SMOW	$\delta^{18}O$ (SMOW) WATER
4418	DMNS 4418 H1E	-5.80	-8.87	21.76	-9.26
4418	DMNS 4418 H2E	-7.39	-8.54	22.11	-8.80
4418	DMNS 4418 H3E	-6.45	-7.81	22.86	-7.82
4418	DMNS 4418 H4E	-7.23	-7.59	23.08	-7.52
4418	DMNS 4418 H5E	-6.50	-8.34	22.31	-8.53
4418	DMNS 4418 H6E	-6.66	-7.78	22.89	-7.78
4418	4418 H6E	-8.27	-9.18	21.44	-9.68
4418	4418 H3E	-9.00	-8.37	22.28	-8.58
4445	PH H3E	-7.20	-8.04	22.62	-8.13
4445	PH H5E	-7.90	-7.77	22.90	-7.76
4445	PH H4E	-7.29	-7.48	23.20	-7.37
4362	MM H1E	-5.77	-8.32	22.33	-8.51
4362	DMNS 4362 H1E	-7.18	-7.23	23.46	-7.03
4362	DMNS 4362 H2E	-6.88	-8.62	22.03	-8.91
4362	DMNS 4362 H3E	-5.45	-7.97	22.70	-8.03
4362	DMNS 4362 H4E	-7.34	-8.08	22.58	-8.18
4362	DMNS 4362 H5E	-5.50	-7.61	23.07	-7.54
4776	4776 H4E	-6.76	-7.47	23.21	-7.36
4776	4776 H5E	-4.92	-8.61	22.04	-8.90
4776	4776 H2E	-7.69	-7.75	22.93	-7.73
4776	4776 H6E	-5.93	-9.20	21.42	-9.71
4776	4776 H1E	-6.46	-7.83	22.84	-7.84
V108/KS-20	KS-20 H1E	-8.52	-8.46	22.19	-8.70
V108/KS-20	KS-20 H2E	-8.25	-9.38	21.24	-9.95
V108/KS-20	KS-20 H3E	-9.46	-7.33	23.36	-7.16
V108/KS-20	KS-20 H4E	-7.54	-9.04	21.59	-9.49
V108/KS-20	KS-20 H5E	-9.36	-8.34	22.31	-8.54
V108/KS-20	UT 14426-H1E	-9.01	-8.80	21.84	-9.16
V108/KS-20	UT 14426-H2E	-8.59	-7.55	23.13	-7.46
V108/KS-20	UT 14426-H3E	-8.65	-7.75	22.92	-7.73
V108/KS-20	UT 14426-H5E	-9.34	-9.61	21.00	-10.26
V108/KS-20	UT 14426-H6E	-8.15	-8.07	22.59	-8.18
V108/KS-20	UT 14426-H7E	-8.80	-8.62	22.03	-8.91

V108/KS-20	UT 14426-H8E	-7.64	-7.10	23.59	-6.85
V108/KS-20	UT 14426-H9E	-8.06	-7.98	22.68	-8.05
V108/KS-20	UT 14426-H10E	-9.14	-8.84	21.80	-9.21

Data from hadrosaur enamel from sites 4418, 4445, 4362, 4776 and V108/KS-20

Site	**Sample ID**	**$\delta^{13}C$ VPDB**	**$\delta^{18}O$ VPDB**	**$\delta^{18}O$ SMOW**	**$\delta^{18}O$ (SMOW) WATER**
4362	DMNS 4362 CR3E	-7.05	-6.57	24.14	-7.34
4362	DMNS 4362 HOR A CR5E	-8.80	-7.85	22.82	-8.42
4362	DMNS 4362 CR2E	-8.84	-8.25	22.41	-8.76
4362	DMNS 4362 HOR A CR6E	-7.54	-9.28	21.34	-9.63
4362	DMNS 4362 CR1E	-5.98	-7.32	23.36	-7.97
4362	DMNS 4362 CR4E	-5.64	-8.70	21.94	-9.14
4778	DMNS 4778 C1E	-9.24	-7.88	22.72	-8.49
4778	DMNS 4778 C2E	-10.20	-6.97	23.67	-7.72
4778	DMNS 4778 CR3E	-8.94	-7.36	23.26	-8.05
4778	DMNS 4778 CR5	-7.44	-7.92	22.68	-8.53
4778	DMNS 4778 CR6E	-9.34	-7.37	23.26	-8.06
4778	DMNS 4778 CR4E	-9.32	-8.03	22.57	-8.62

Data from crocodile enamel from sites 4362 and 4778

Site	**Sample ID**	**$\delta^{13}C$ VPDB**	**$\delta^{18}O$ VPDB**	**$\delta^{18}O$ SMOW**	**$\delta^{18}O$ (SMOW) WATER**
4445	PH4445-MIC1	-6.97	-11.38	19.18	-8.97
4445	PH4445-MIC2	-6.56	-11.02	19.55	-8.60
4445	PH4445-MIC3	-6.69	-11.06	19.51	-8.65
4445	PH4445-MIC4	-6.51	-10.49	20.10	-8.05
4362	4362 MME MIC1	-6.35	-11.43	19.12	-9.03
4362	4362 MME MIC2	-6.88	-11.42	19.14	-9.02
4362	4362 MME MIC3	-6.95	-11.48	19.08	-9.07
4362	4362 MME MIC4	-6.62	-11.55	19.00	-9.15

Data from micrites from sites 4445 and 4362

Site	Sample ID	$\delta^{13}C$ VPDB	$\delta^{18}O$ VPDB	$\delta^{18}O$ SMOW	$\delta^{18}O$ (SMOW) WATER
4418	EKP-4418-N1-51/FRICKE/K850	-6.64	-8.44	22.21	-5.94
4418	EKP-4418-N2-52/FRICKE/K850	-9.19	-7.79	22.88	-5.28
4418	EKP-4418-N3-53/FRICKE/K850	-7.19	-7.91	22.75	-5.40
4418	4418-N3	-7.94	-8.66	21.98	-6.17
4418	4418-N5	-7.59	-8.33	22.32	-5.83
4418	4418-N6	-8.15	-7.70	22.97	-5.18
4445	EKP-PH-N2-71/FRICKE/K850	-10.31	-6.94	23.75	-4.40
4445	EKP-PH-N3-72/FRICKE/K850	-10.50	-6.90	23.80	-4.36
4445	73 11-2-15B/FRICKE/K874	-10.35	-7.20	23.49	-4.67
4445	74 11-2-15B/FRICKE/K874	-10.36	-6.74	23.96	-4.20
4445	75 11-2-15B/FRICKE/K874	-10.60	-7.64	23.03	-5.12
4445	76 11-2-15B/FRICKE/K874	-10.31	-7.03	23.66	-4.49
4776	EKP-TT-N1-1/FRICKE/K850	-8.63	-7.79	22.88	-5.27
4776	EKP-TT-N2-2/FRICKE/K850	-8.65	-7.31	23.38	-4.78
4776	EKP-TT-N3-3/FRICKE/K850	-9.21	-7.49	23.18	-4.97
4776	4 11-2-15B/FRICKE/K874	-8.79	-7.34	23.34	-4.81
4776	5 11-2-15B/FRICKE/K874	-9.19	-9.27	21.35	-6.80
4776	6 11-2-15B/FRICKE/K874	-8.57	-8.27	22.38	-5.77
4776	7 11-2-15B/FRICKE/K874	-9.21	-7.80	22.87	-5.28
4776	8 11-2-15B/FRICKE/K874	-8.69	-8.53	22.12	-6.03
V108/KS-20	EKP-V108L-N1-44/FRICKE/K850	-9.70	-7.50	23.17	-4.98
V108/KS-21	EKP-V108L-N2-45/FRICKE/K850	-9.18	-8.06	22.60	-5.55
V108/KS-22	EKP-V108L-N3-46/FRICKE/K850	-9.79	-7.88	22.79	-5.37
V108/KS-23	EKP-V108U-N1-49/FRICKE/K850	-10.14	-7.89	22.78	-5.37
V108/KS-24	EKP-V108U-N2-50/FRICKE/K850	-11.17	-7.70	22.97	-5.18
V108/KS-25	K20-2-N1	-9.94	-7.50	23.17	-4.98
V108/KS-26	K20-2-N2	-9.59	-7.61	23.06	-5.09
V108/KS-27	K20-2-N3	-9.77	-7.81	22.86	-5.30
V108/KS-28	K20-2-N4	-9.65	-7.29	23.40	-4.76
V108/KS-29	K20-2-N5	-10.24	-7.91	22.75	-5.40

Data from pedogenic carbonate nodules from sites 4418, 4445, 4776 and V208/KS-20

Site	Sample ID	$\delta^{13}C$ VPDB	$\delta^{18}O$ VPDB	$\delta^{18}O$ SMOW
4418	DMNS 4418 H1D	-6.86	-8.75	21.89
4418	DMNS 4418 H2D	-7.24	-8.73	21.91
4418	DMNS 4418 H4D	-7.03	-9.47	21.15
4418	DMNS 4418 H5D	-2.23	-8.23	22.43
4418	DMNS 4418 H6D	-3.04	-8.81	21.83
4418	EKP4418-H1D-124/FRICKE/K850	-4.20	-7.99	22.68
4418	EXP4418-H2D-125/FRICKE/K850	-5.43	-7.99	22.67
4418	EKP4418-H3D-126/FRICKE/K850	-5.71	-8.20	22.45
4445	EKP-PH-H4D-113/FRICKE/K850	-3.51	-7.58	23.09
4445	EKP-PH-H5D-114/FRICKE/K850	-0.95	-7.41	23.27
4362	DMNS 4362 H1D	-2.55	-7.70	22.97
4362	DMNS 4362 H2D	-6.83	-8.51	22.14
4362	DMNS 4362 H4D	-4.48	-8.07	22.59
4362	DMNS 4362 H5D	1.13	-7.74	22.93
4362	EKP-MME-H1D-107/FRICKE/K850	1.38	-7.92	22.74
4362	EKP-MME-H2D-109/FRICKE/K850	0.55	-7.23	23.45
4362	EKP-MM-H1D-105/FRICKE/K850	-1.58	-7.48	23.20
4362	EKP-MM-H2D-106/FRICKE/K850	-2.24	-7.88	22.78
V108/KS-20	KS-20 H1D	-7.06	-9.24	21.39
V108/KS-20	KS-20 H2D	-4.95	-7.99	22.67
V108/KS-20	KS-20 H3D	-9.01	-8.45	22.20
V108/KS-20	KS-20 H4D	-6.32	-8.70	21.94
V108/KS-20	KS-20 H5D	-9.04	-8.65	21.99
V108/KS-20	UT 14426-H1D	-7.37	-8.59	22.06
V108/KS-20	UT 14426-H2D	-7.36	-8.29	22.36
V108/KS-20	UT 14426-H3D	-5.99	-8.62	22.02
V108/KS-20	UT 14426-H4D	-5.67	-8.52	22.13
V108/KS-20	UT 14426-H5D	-7.89	-9.90	20.70
V108/KS-20	UT 14426-H6D	-6.86	-8.36	22.30
V108/KS-20	UT 14426-H7D	-8.32	-8.02	22.65
V108/KS-20	UT 14426-H8D	-4.28	-7.64	23.04
V108/KS-20	UT 14426-H9D	-5.72	-8.30	22.36
V108/KS-20	UT 14426-H10D	-8.46	-8.32	22.33

Data from hadrosaur dentine from sites 4418, 4445, 4362 and V108/KS-20

APPENDIX 2

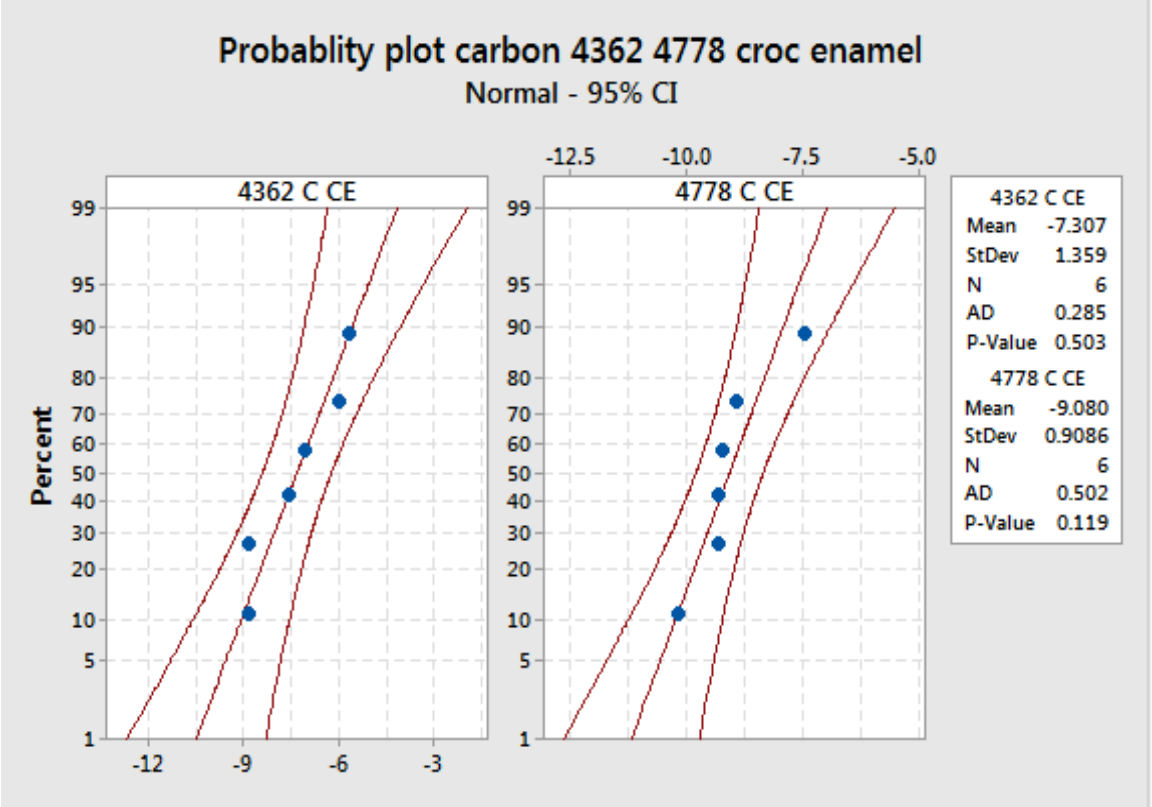

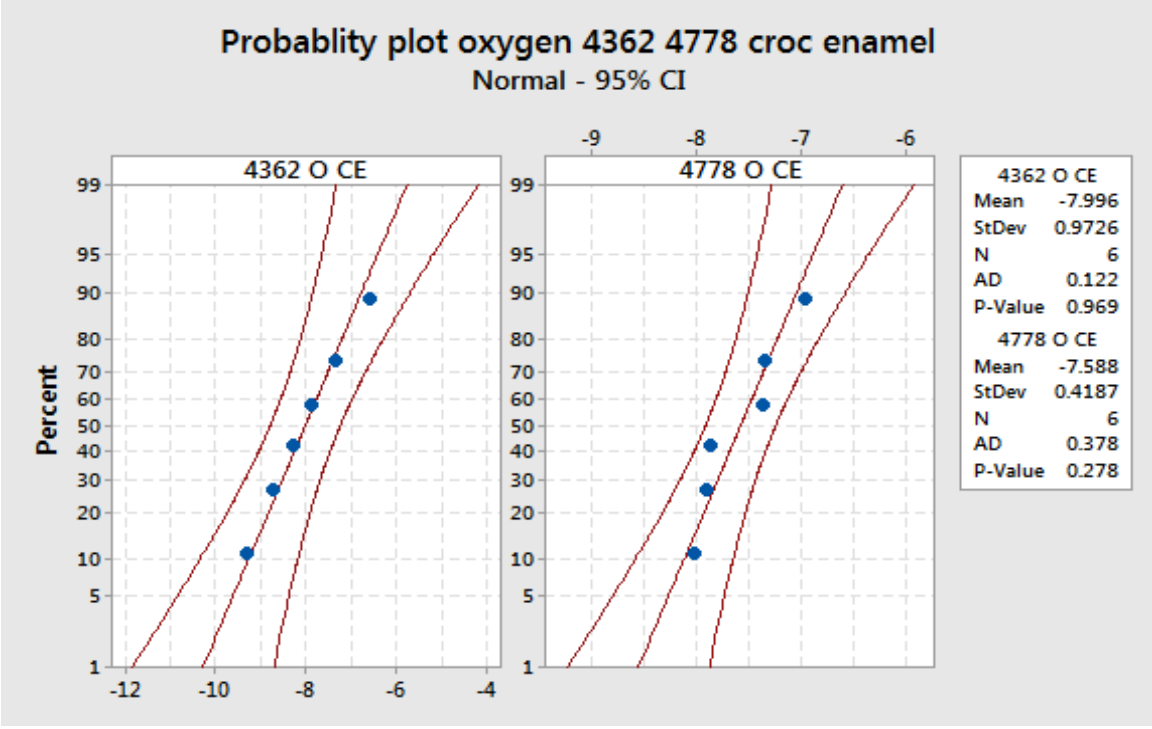

Top: Probability plots, Anderson-Darling values, associated P-values, means and standard deviations for carbon ϱ13C for crocodile enamel from sites 4362 and 4778. **Bottom**: Probability plots, Anderson-Darling values, and P-values for ϱ18O for crocodile enamel from sites 4362 and 4778.

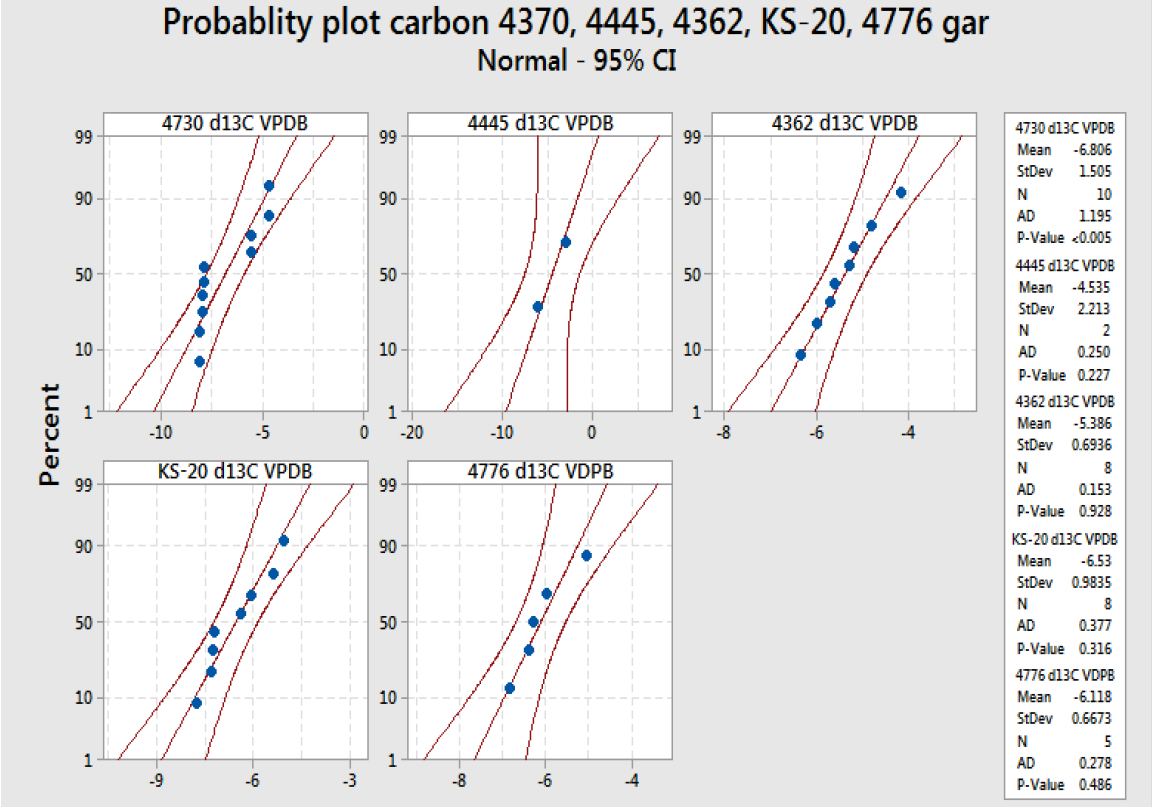

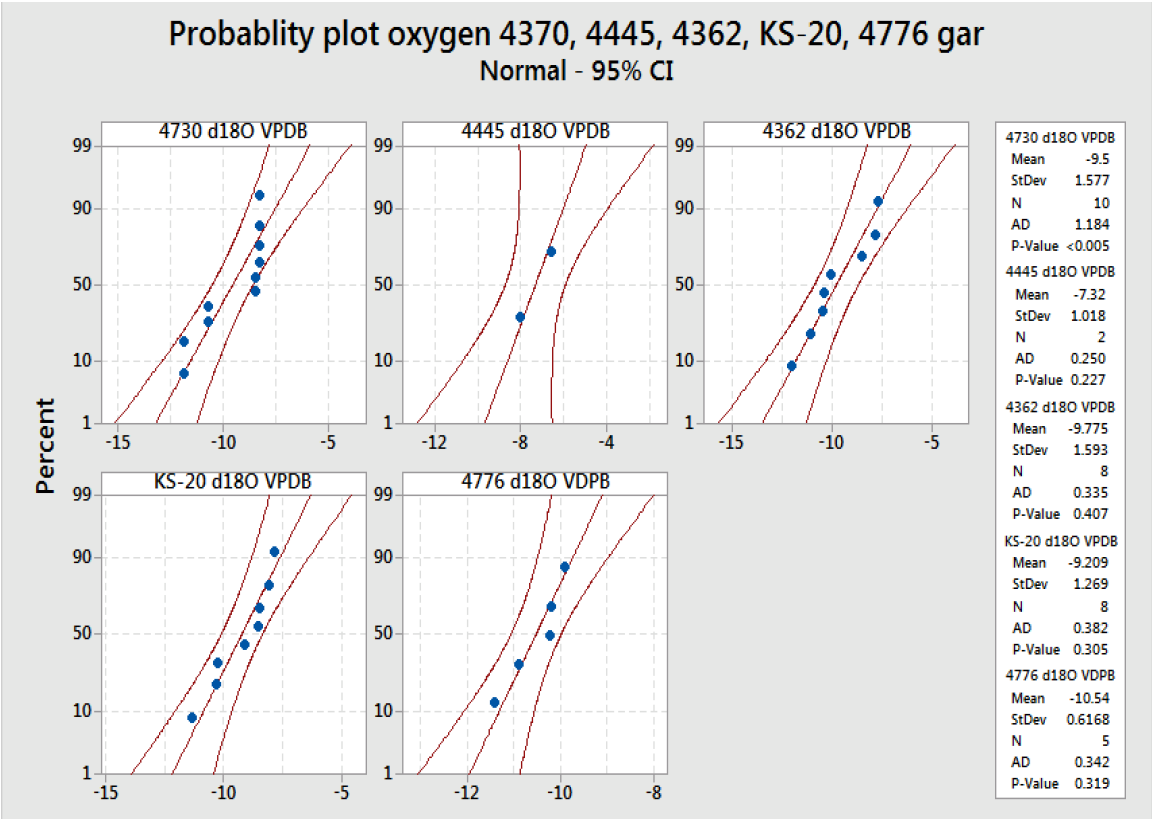

Top: Probability plots, Anderson-Darling values, associated P-values, means and standard deviations for carbon values for gar (ganonie) from sites 4730, 4445, 4362, KS-20 and 4776. **Bottom:** Same data for same sites for oxygen values.

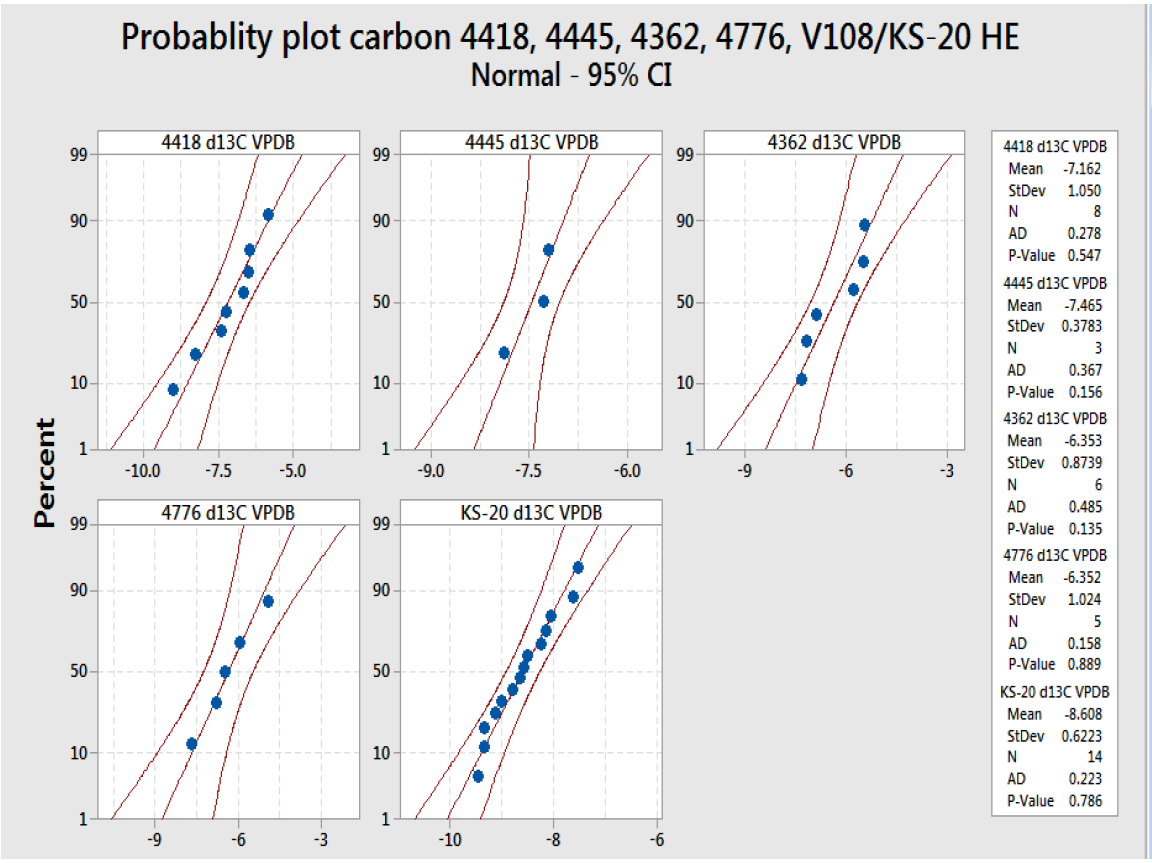

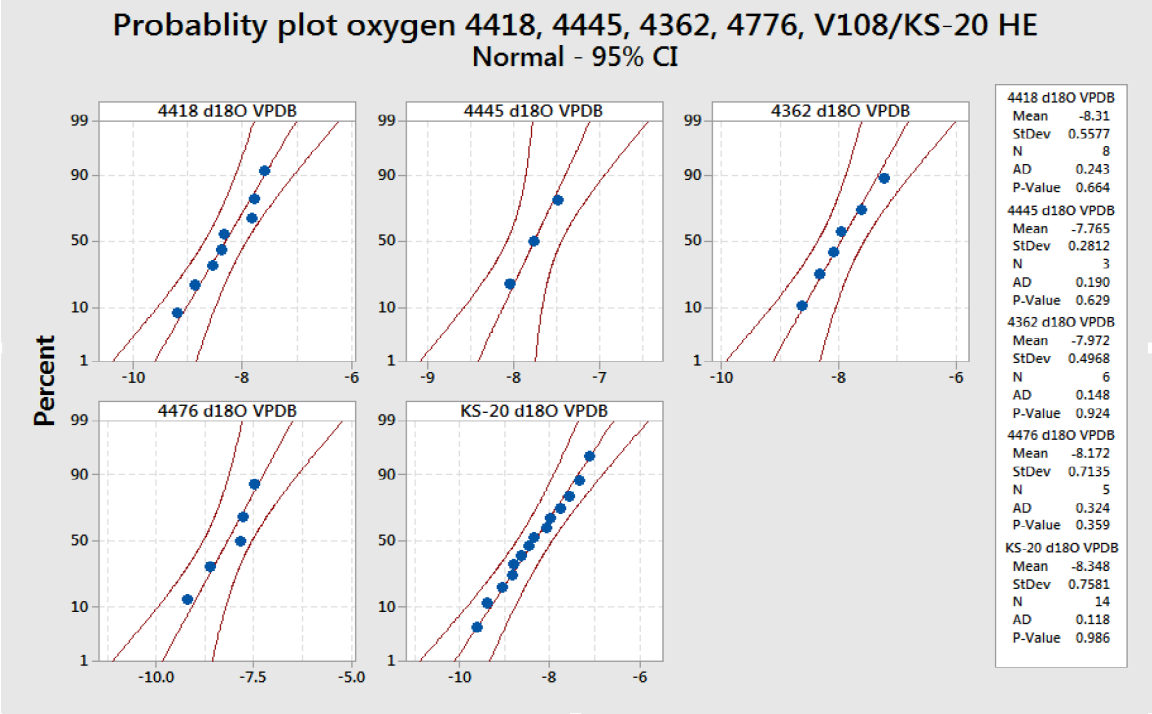

Top: Probability plots, Anderson-Darling values, associated P-values, means and standard deviations for carbon values for hadrosaur enamel from sites 4418, 4445, 4362, 4776, V108/KS-20. **Bottom**: same data for same sites for oxygen values.

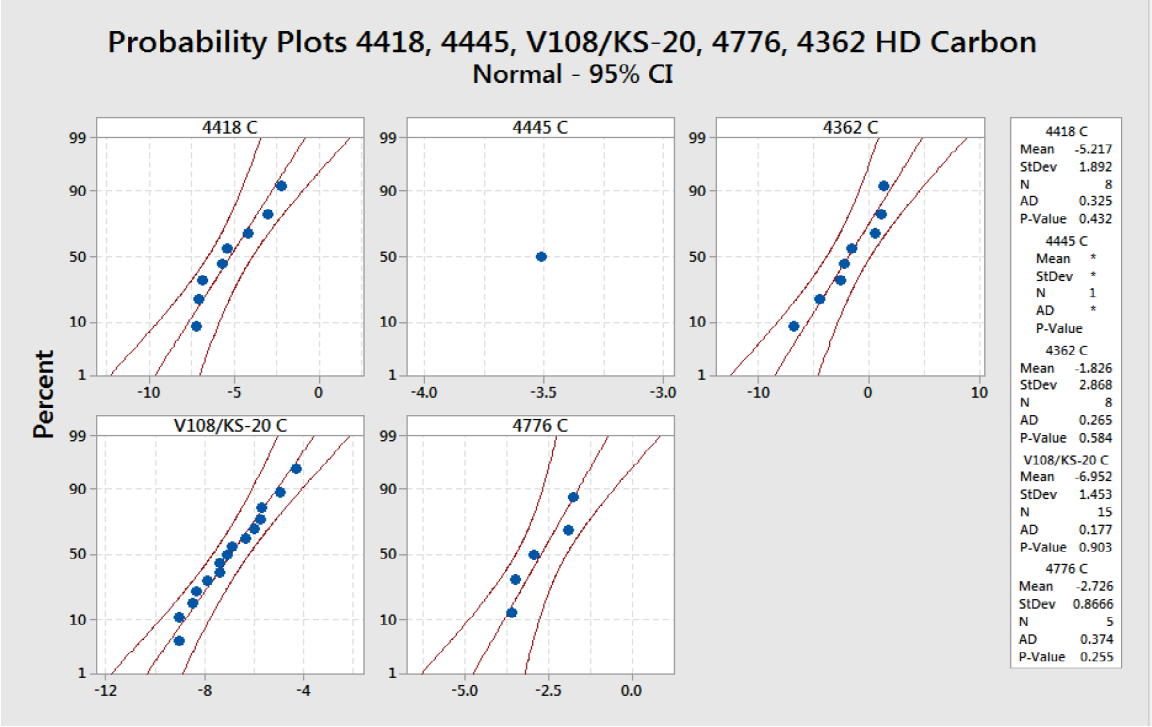

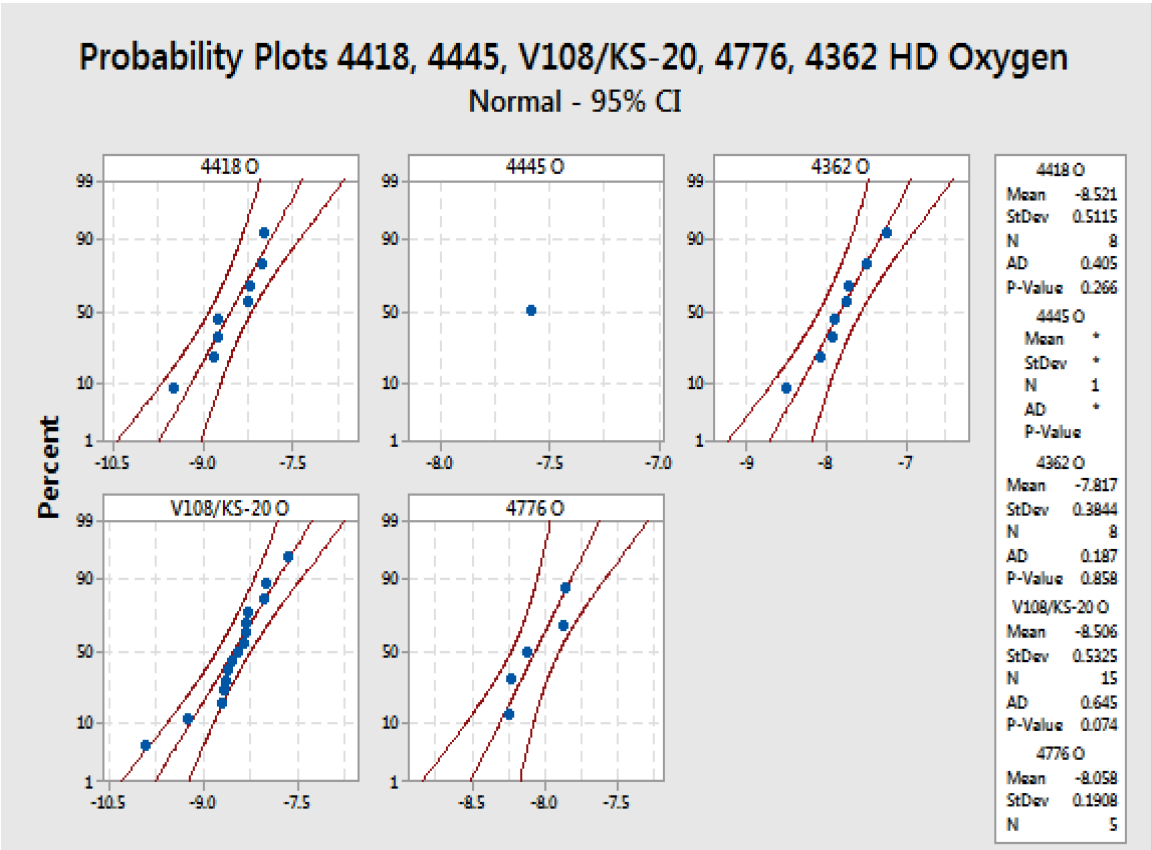

Top: Probability plots, Anderson-Darling values, associated P-values, means and standard deviations for carbon values for hadrosaur dentine from sites 4418, 4445, 4362, 4776, V108/KS-20. **Bottom**: same data for same sites for oxygen values.

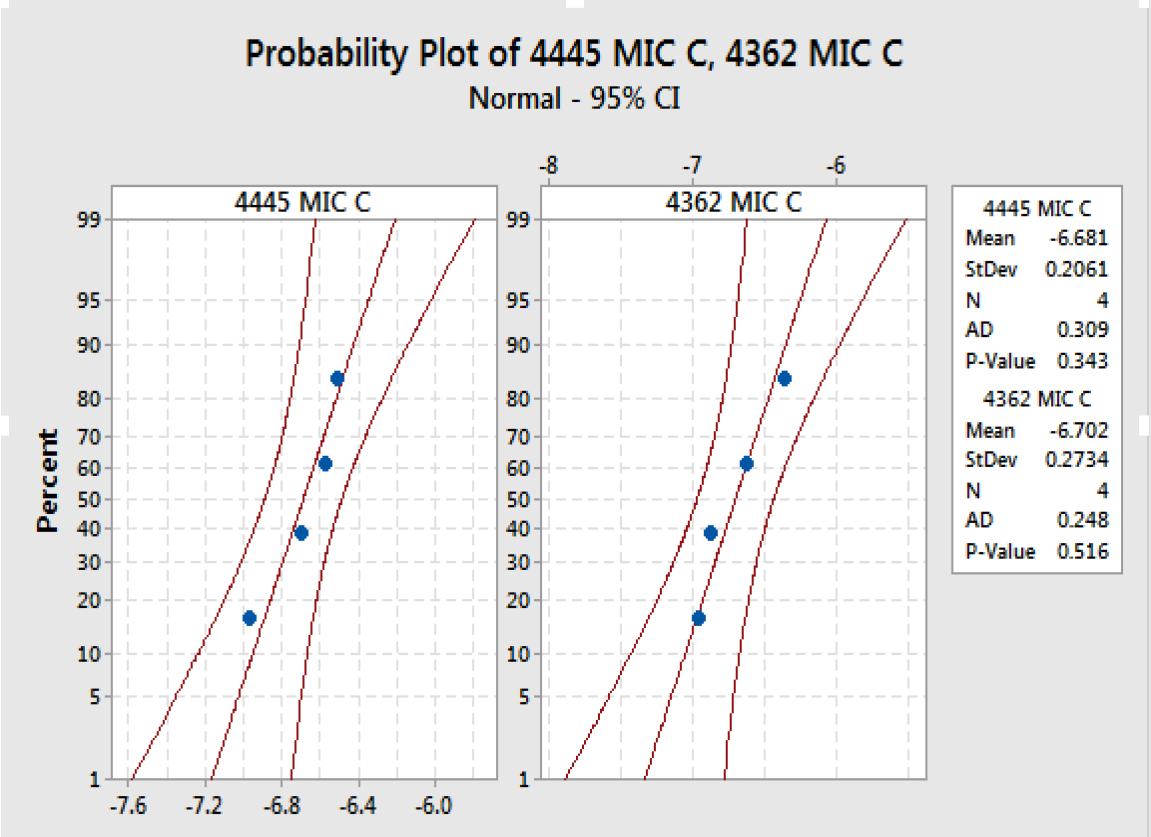

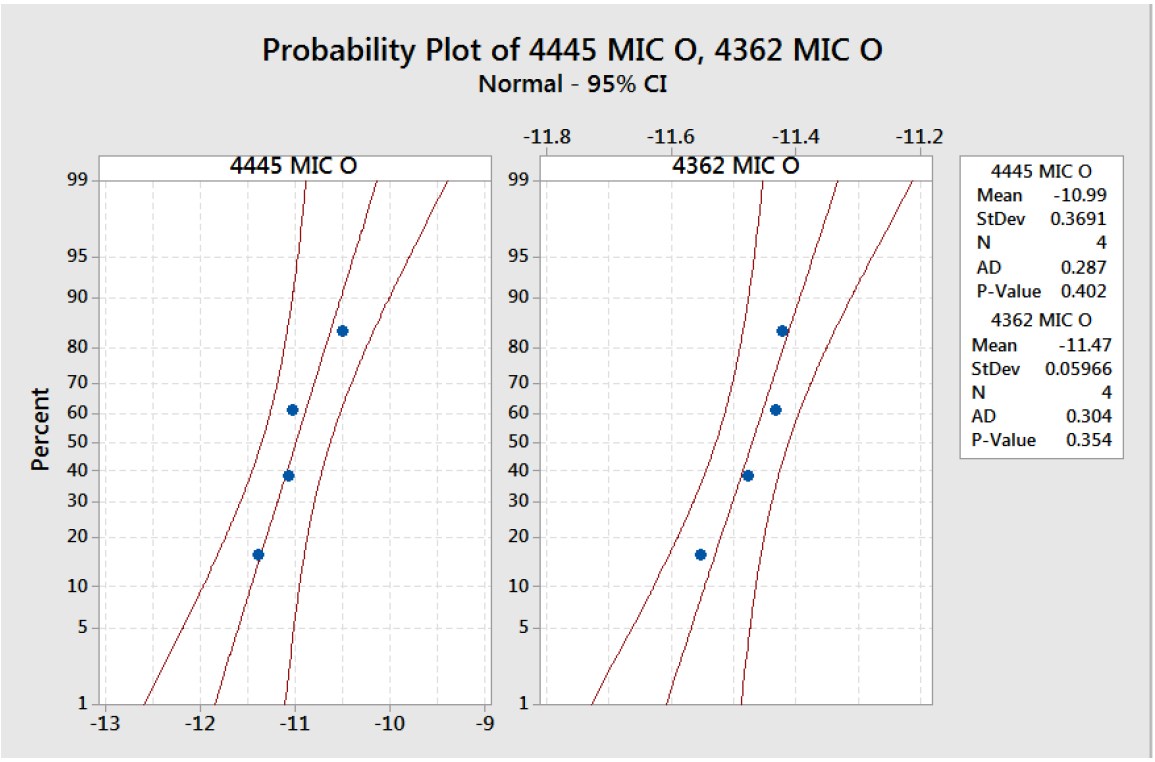

Top: Probability plots, Anderson-Darling values, associated P-values, means and standard deviations for carbon values for hadrosaur dentine from sites 4445 and 4362 for ponded carbonates. **Bottom:** Same data for same sites but for oxygen values.

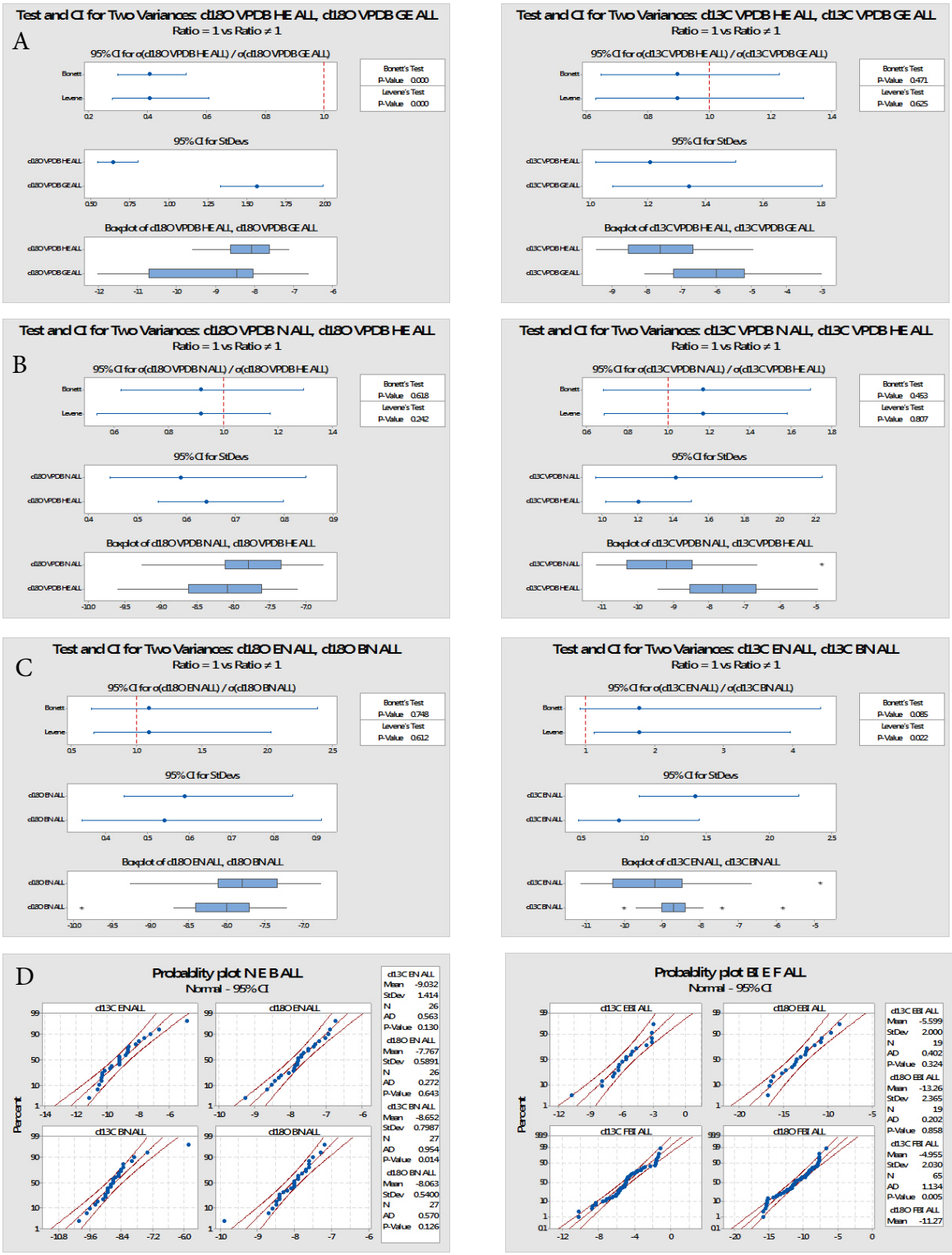

A: Tests and confidence intervals for difference in variances for hadrosaur enamel against gar ganonie for oxygen and carbon. **B:** Test and confidence intervals for variance for nodule data against hadrosaur enamel for carbon and oxygen. **C:** Test and confidence intervals for variance for nodules in this study against those included in Foreman et al (2015). **D:** Normal probability plots for nodules and bivalves included in Foreman et al (2015).

APPENDIX 3

Variable 1	Variable 2	P value	T test conclusion
Hadrosaur Dentine All Carbon	Hadrosaur Enamel All Carbon	9.3376E-07	Significant
Hadrosaur Dentine All Oxygen	Hadrosaur Enamel All Oxygen	0.729160672	Not Significant
4362 Hadrosaur Dentine Carbon	4362 Hadrosaur Enamel Carbon	0.000625833	Significant
4362 Hadrosaur Dentine Oxygen	4362 Hadrosaur Enamel Oxygen	0.011608703	Significant
4776 Hadrosaur Dentine Carbon	4776 Hadrosaur Enamel Carbon	0.000309042	Significant
4776 Hadrosaur Dentine Oxygen	4776 Hadrosaur Enamel Oxygen	0.747287789	Not Significant
V108/KS-20 Hadrosaur Dentine Carbon	V108/KS-20 Hadrosaur Enamel Carbon	0.000718093	Significant
V108/KS-20 Hadrosaur Dentine Carbon	V108/KS-20 Hadrosaur Enamel Oxygen	0.524605921	Not Significant
4418 Hadrosaur Dentine Carbon	4418 Hadrosaur Enamel Carbon	0.027368767	Not Significant
4418 Hadrosaur Dentine Carbon	4418 Hadrosaur Enamel Oxygen	0.442970129	Not Significant
Hadrosaur Dentine All Carbon	Pedogenic Carbonates All Carbon	6.42907E-12	Significant
Hadrosaur Dentine All Oxygen	Pedogenic Carbonates All Oxygen	0.000215615	Significant
4776 Hadrosaur Dentine Carbon	4776 Pedogenic Carbonates Carbon	2.13391E-05	Significant
4776 Hadrosaur Dentine Oxygen	4776 Pedogenic Carbonates Oxygen	0.751824663	Not Significant
V108/KS-20 Hadrosaur Dentine Carbon	V108/KS-20 Pedogenic Carbonates Carbon	7.60685E-07	Significant
V108/KS-20 Hadrosaur Dentine Oxygen	V108/KS-20 Pedogenic Carbonates Oxygen	6.61878E-36	Significant
4418 Hadrosaur Dentine Carbon	4418 Pedogenic Carbonates Carbon	0.007021364	Significant
4418 Hadrosaur Dentine Oxygen	4418 Pedogenic Carbonates Oxygen	0.137927714	Not Significant
Hadrosaur Enamel All Carbon	Pedogenic Carbonates All Carbon	2.65469E-08	Significant
Hadrosaur Enamel All Oxygen	Pedogenic Carbonates All Oxygen	0.002668025	Not Significant

4776 Hadrosaur Enamel Carbon	4776 Pedogenic Carbonates Carbon	0.005834948	Significant
4776 Hadrosaur Enamel Oxygen	4776 Pedogenic Carbonates Oxygen	0.637509217	Not Significant
V108/KS-20 Hadrosaur Enamel Carbon	V108/KS-20 Pedogenic Carbonates Carbon	1.71174E-05	Significant
V108/KS-20 Hadrosaur Enamel Oxygen	V108/KS-20 Pedogenic Carbonates Oxygen	0.010115424	Significant
4418 Hadrosaur Enamel Carbon	4418 Pedogenic Carbonates Carbon	0.254686089	Not Significant
4418 Hadrosaur Enamel Oxygen	4418 Pedogenic Carbonates Oxygen	0.507125387	Not Significant
4445 Hadrosaur Enamel Carbon	4445 Pedogenic Carbonates Carbon	0.07080967	Significant
4445 Hadrosaur Enamel Oxygen	4445 Pedogenic Carbonates Oxygen	0.027504331	Significant
Gar Ganonie All Carbon	Hadrosaur Enamel All Carbon	3.33043E-05	Significant
Gar Ganonie All Oxygen	Hadrosaur Enamel All Oxygen	0.000724179	Significant
4362 Gar Ganonie Carbon	4362 Hadrosaur Enamel Carbon	0.052514265	Significant
4362 Gar Ganonie Oxygen	4362 Hadrosaur Enamel Oxygen	0.014570447	Not Significant
V108/KS-20 Gar Ganonie Carbon	V108/KS-20 Hadrosaur Enamel Carbon	9.47072E-05	Significant
V108/KS-20 Gar Ganonie Oxygen	V108/KS-20 Hadrosaur Enamel Oxygen	0.213745645	Not Significant
4445 Gar Ganonie Carbon	4445 Hadrosaur Enamel Carbon	0.283792652	Not Significant
4445 Gar Ganonie Oxygen	4445 Hadrosaur Enamel Oxygen	0.599975062	Not Significant
Mode 1 Gar Ganonie All Carbon	Mode 2 Gar Ganonie All Carbon	0.220667783	Not Significant
Mode 1 Gar Ganonie All Oxygen	Mode 2 Gar Ganonie All Oxygen	6.02956E-07	Significant
4362 Mode 1 Gar Ganonie Carbon	4362 Mode 2 Gar Ganonie Carbon	0.09244403	Significant
4362 Mode 1 Gar Ganonie Oxygen	4362 Mode 2 Gar Ganonie Oxygen	0.053650722	Significant

V108/KS-20 Mode 1 Gar Ganonie Carbon	V108/KS-20 Mode 2 Gar Ganonie Carbon	0.42203828	Not Significant
V108/KS-20 Mode 1 Gar Ganonie Oxygen	V108/KS-20 Mode 2 Gar Ganonie Oxygen	0.006769109	Significant
4730 Mode 1 Gar Ganonie Carbon	4730 Mode 2 Gar Ganonie Carbon	0.09151749	Significant
4730 Mode 1 Gar Ganonie Oxygen	4730 Mode 2 Gar Ganonie Oxygen	0.065152748	Significant
4362 Crocodile Enamel Carbon	4778 Crocodile Enamel Carbon	0.132446021	Not Significant
4362 Crocodile Enamel Oxygen	4778 Crocodile Enamel Oxygen	0.376618807	Not Significant
Foreman et al (2015) Nodules Carbon	Evans Nodules Carbon	0.917661531	Not Significant
Foreman et al (2015) Nodules Oxygen	Evans Nodules Oxygen	0.357935817	Not Significant
4445/4362 Micrites Carbon	All Nodules Carbon	1.35163E-11	Significant
4445/4362 Micrites Oxygen	All Nodules Oxygen	7.29692E-14	Significant
Bivalves 365/325 Carbon	Bivalves 315/455 Carbon	0.024004587	Significant
Bivalves 365/325 Oxygen	Bivalves 315/455 Oxygen	0.042856976	Significant

APPENDIX 4

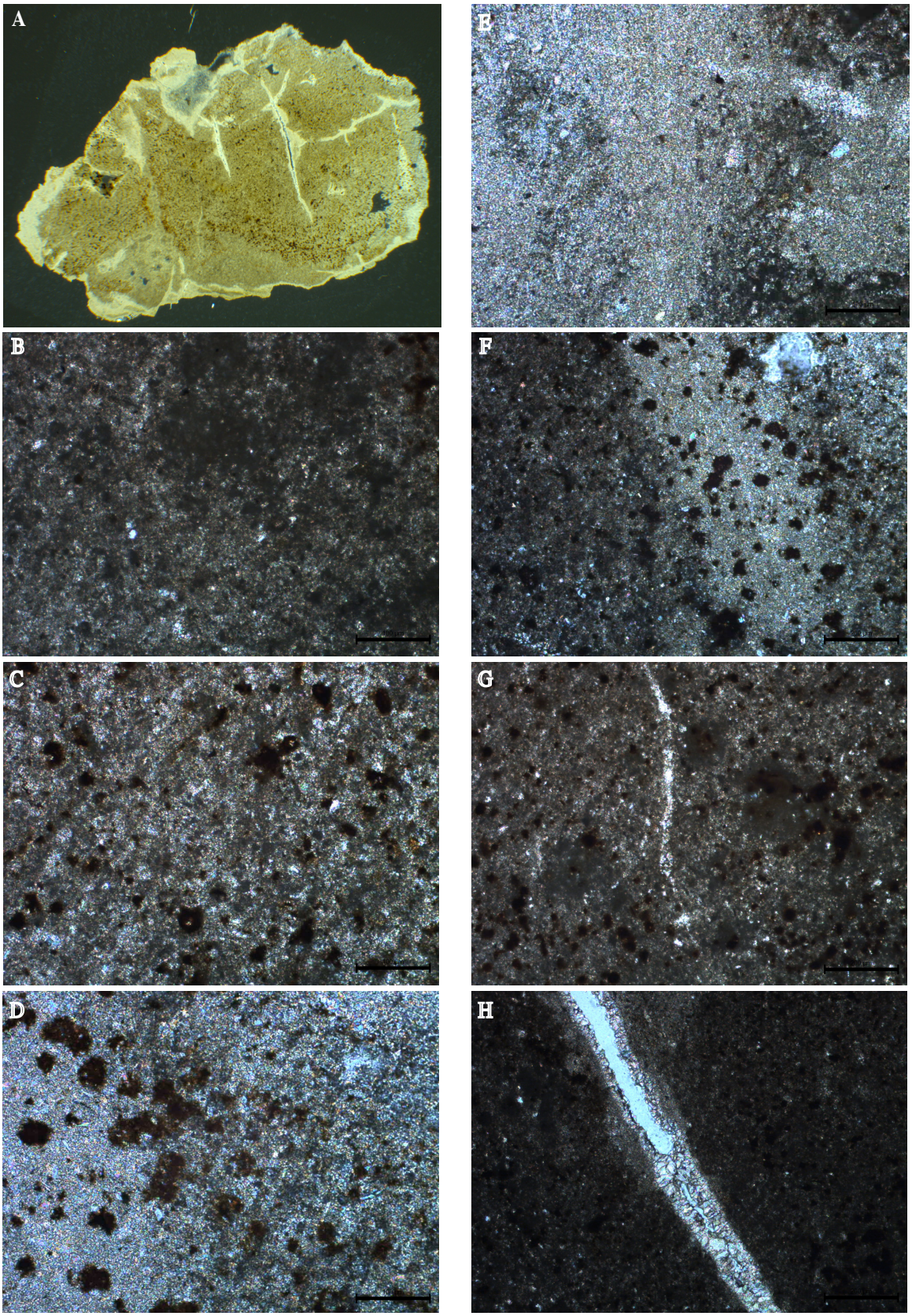

A) Whole nodule image of N2 (4370) B) center of N2 4370 C) center of N2 4370 D) edge of N2 4370 E) edge of N2 (4370) F) edge of N2 4370 G) veins of N2 4370 H) veins of N2 4370

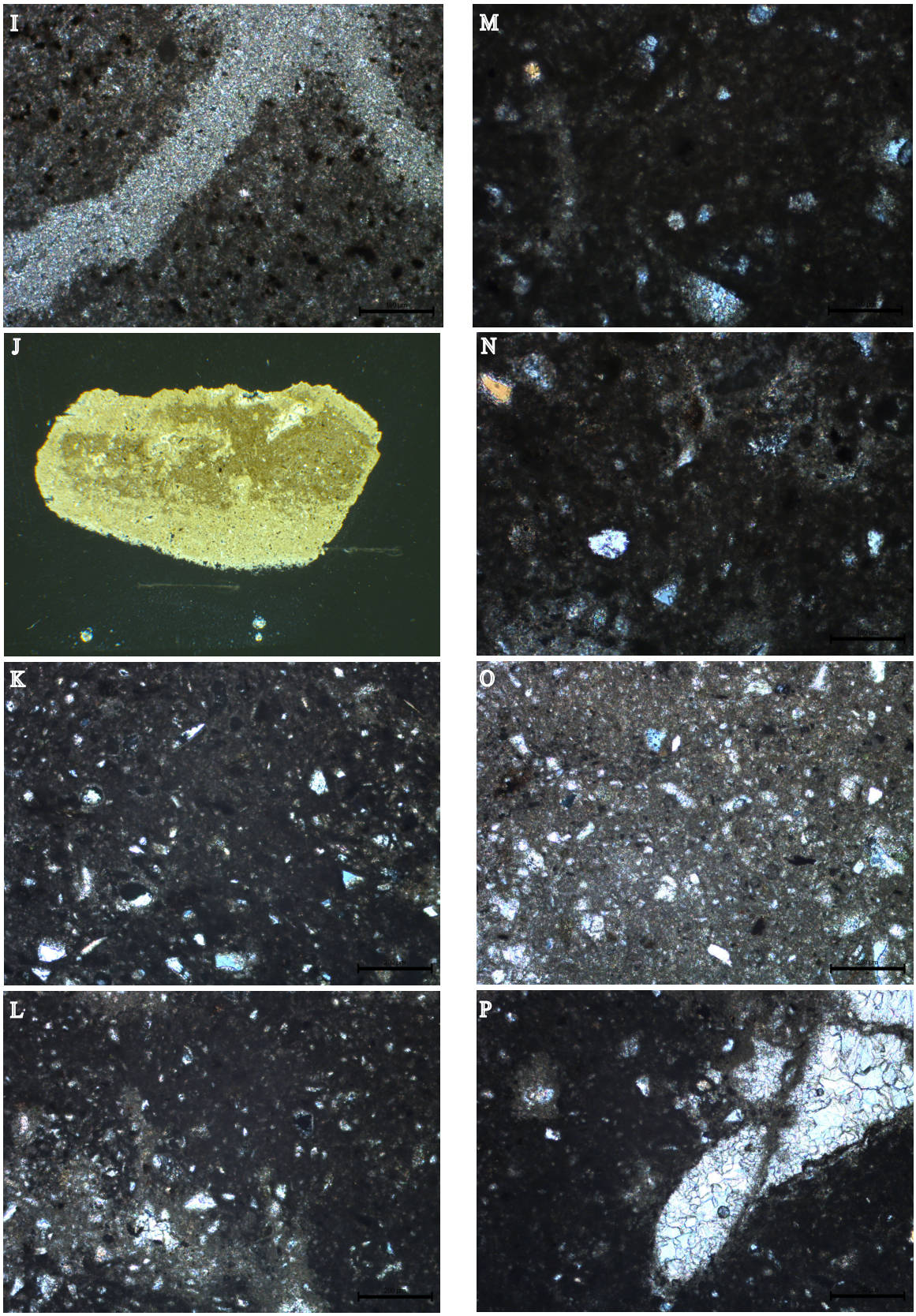

I) Veins of N2 (4370) J) whole nodules of N3 4370 K) center of N3 4370 L) center of N3 4370 M) center of N3 (4370) N) center of N3 4370 O) edge of N3 4370 P) vug of N3 4370

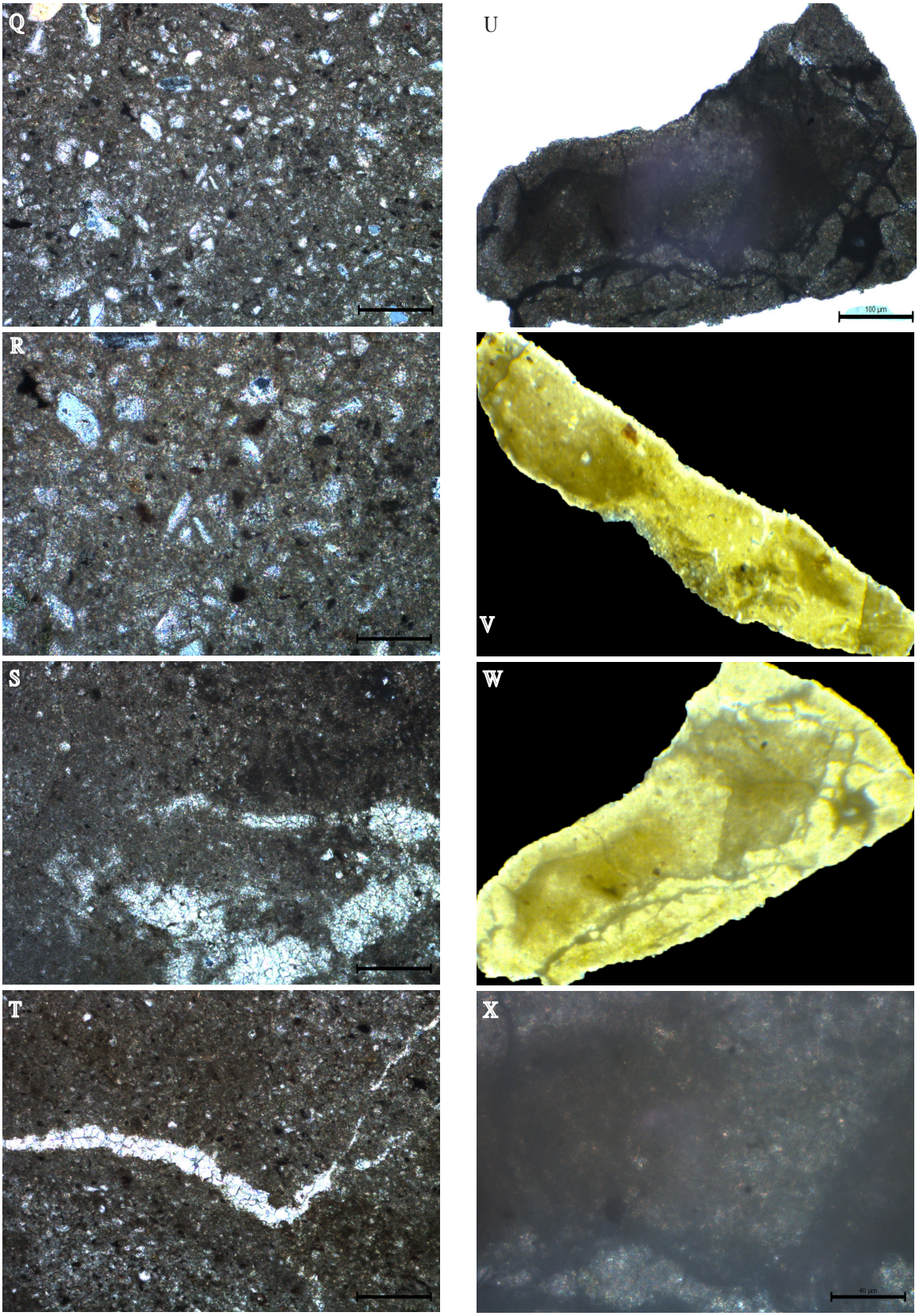

Q) Edge of N3 (4370) R) edge of N3 4370 S) vug of N1 4418 T) vug/vein of N1 4418 U) whole nodule of N3 4418 V) whole nodule of N3 4418 W) whole nodule of N3 4418 X) center of N3 4418

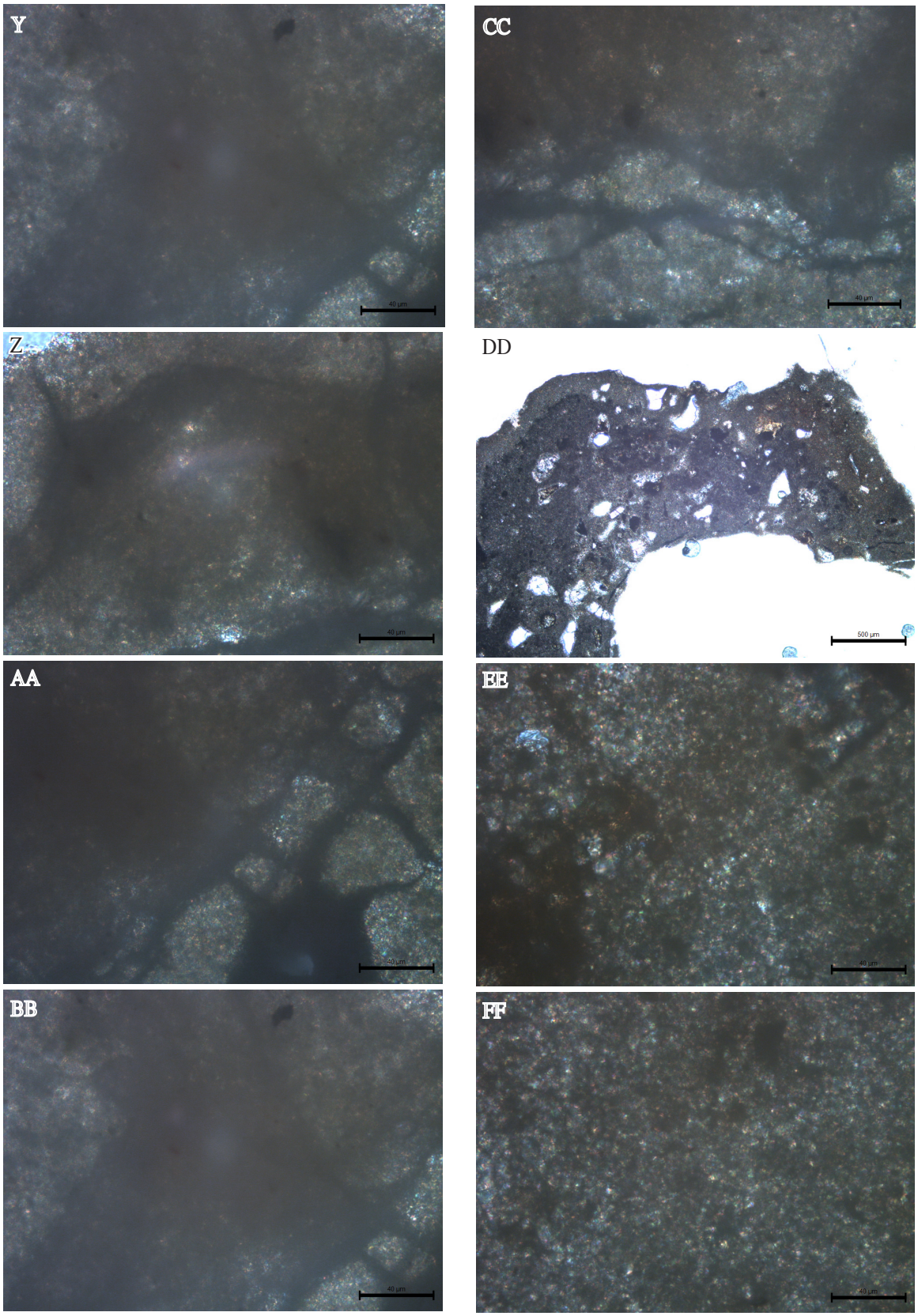

Y) Center of N3 4418 Z) center of N3 4418 AA) edge of N3 4418 BB) edge of N3 4418 CC) edge of N3 4418 DD) whole nodule N2 4445 EE) center of N2 4445 FF) center of N2 4445

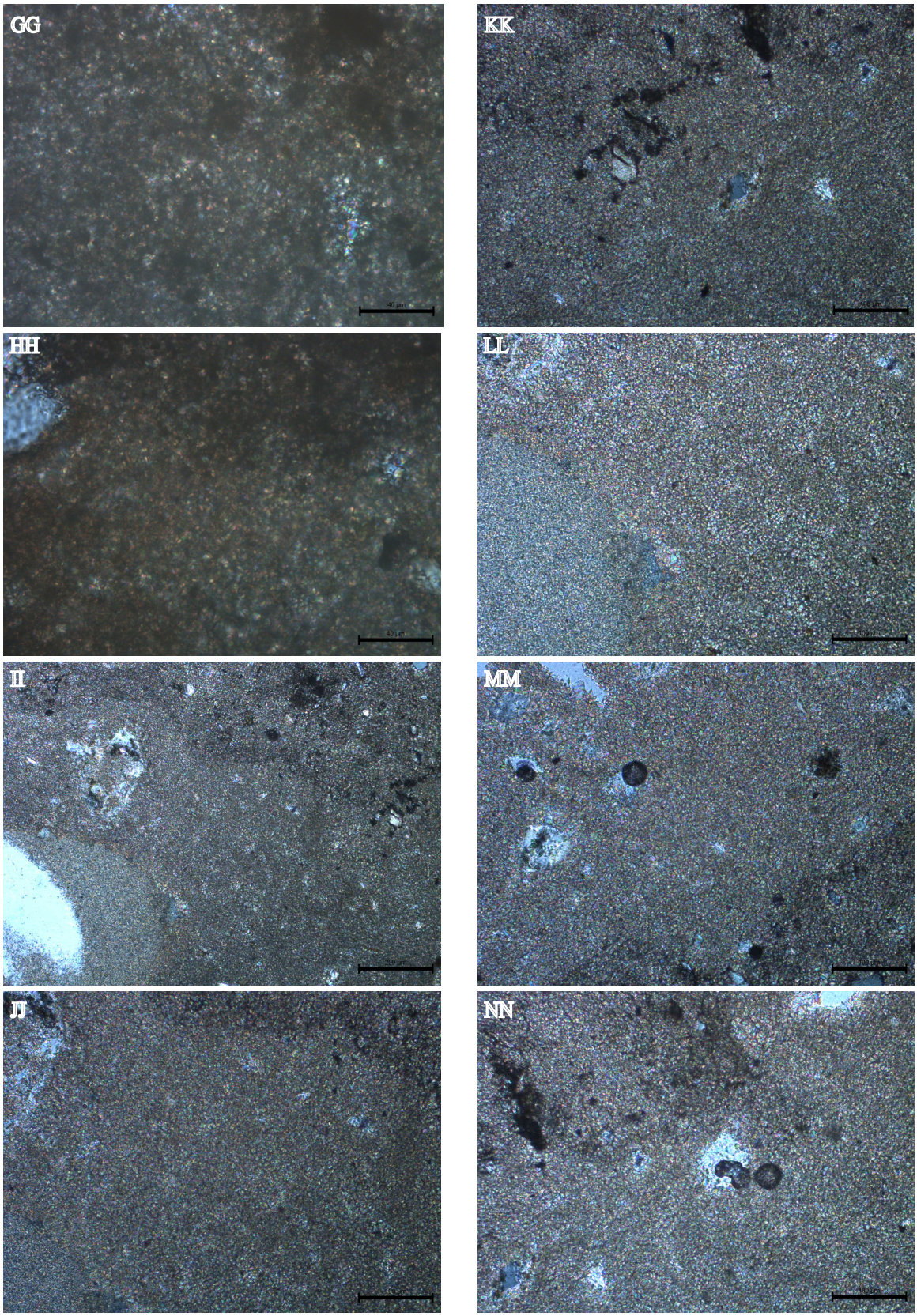

GG) Edge of N2 4445 HH) edge of N2 4445 II) center of N3 4445 JJ) center of N3 4445 KK) center of N3 4445 LL) center of N3 4445 MM) center of N3 4445 NN) center of N3 4445

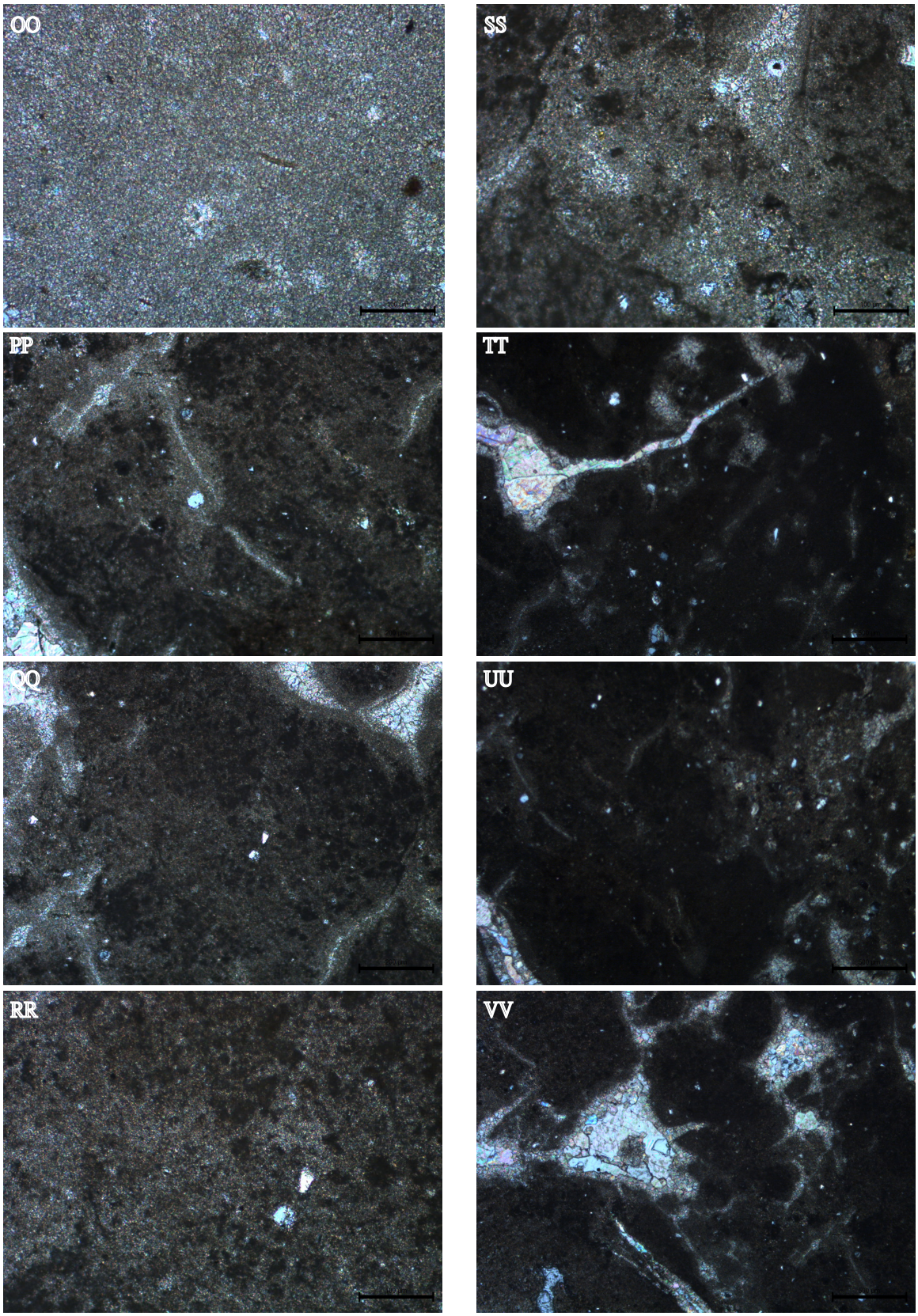

OO) Center of N3 4445 PP) center of N1 4776 QQ) center of N1 4776 RR) center of N1 4776 SS) center of N1 4776 TT) edge of N1 4776 UU) veins N1 4776 VV) veins N1 4776

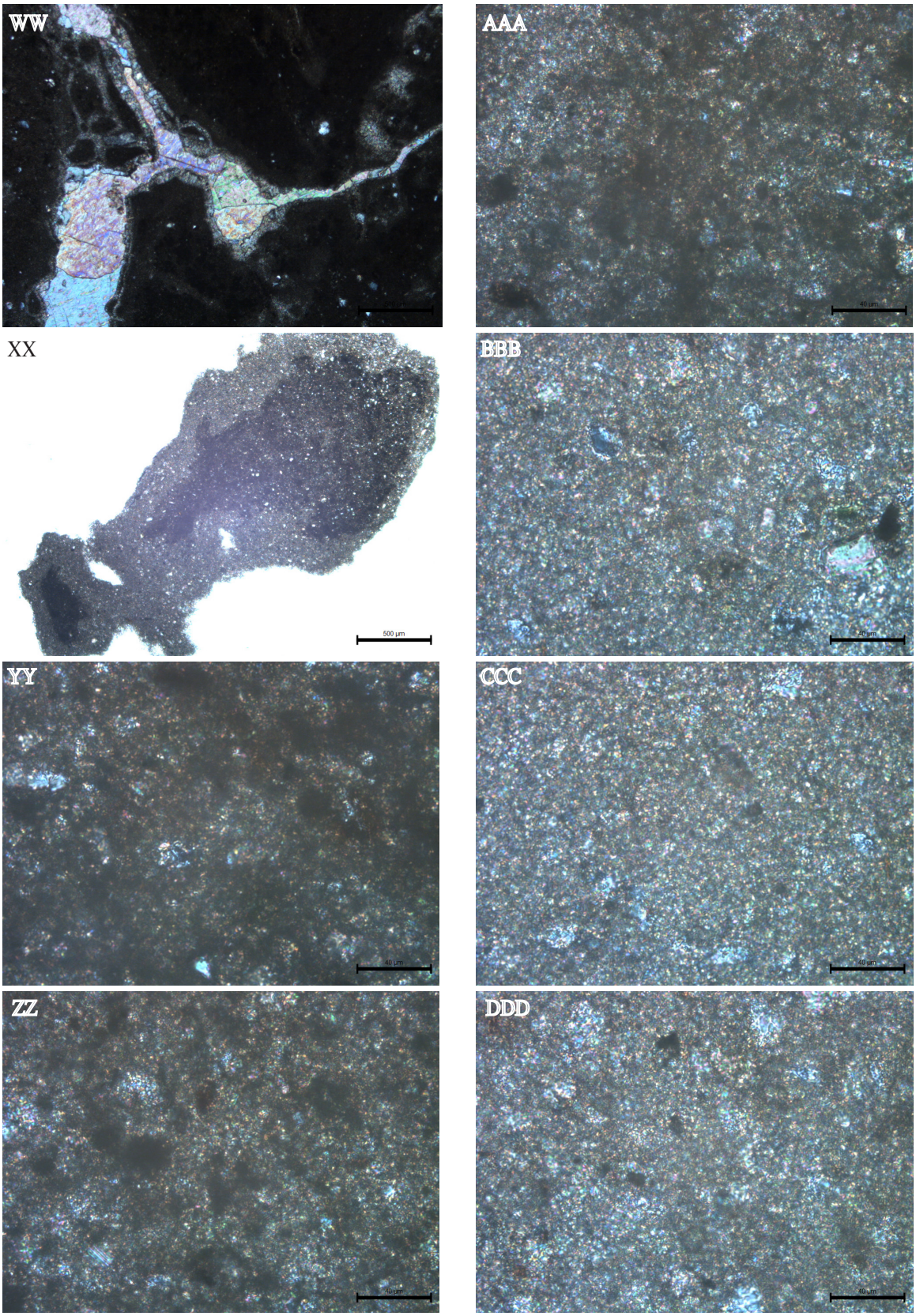

WW) Veins N1 4776 XX) whole nodule N2 4776 YY) center N2 4776 ZZ) center N2 4776 AAA) center of N2 4776 BBB) edge of N2 4776 CCC) edge of N2 4776 DDD) edge of N2 4776

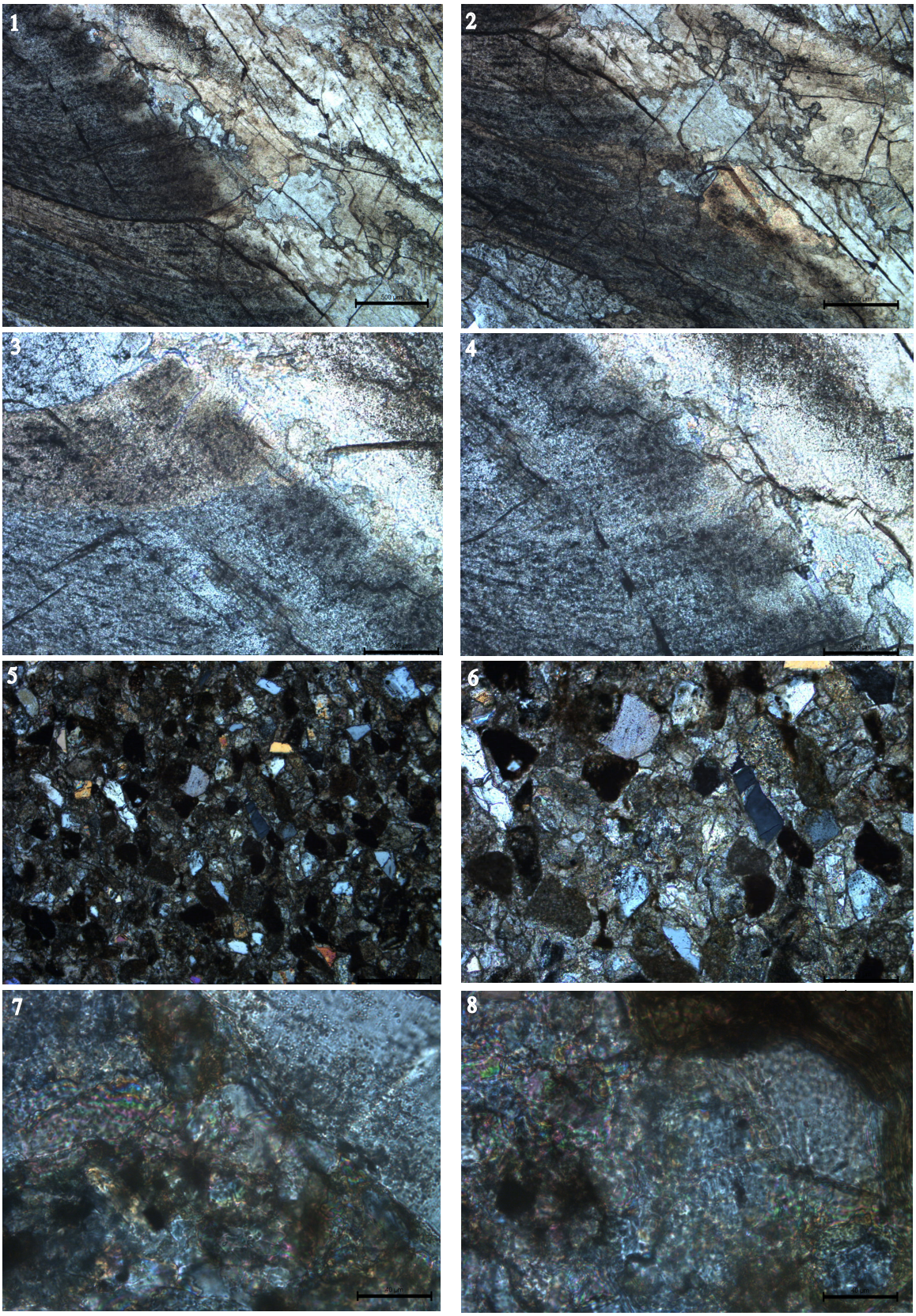

1-4) Bivalve material from Bivalve Site 5-8) cement from the same site

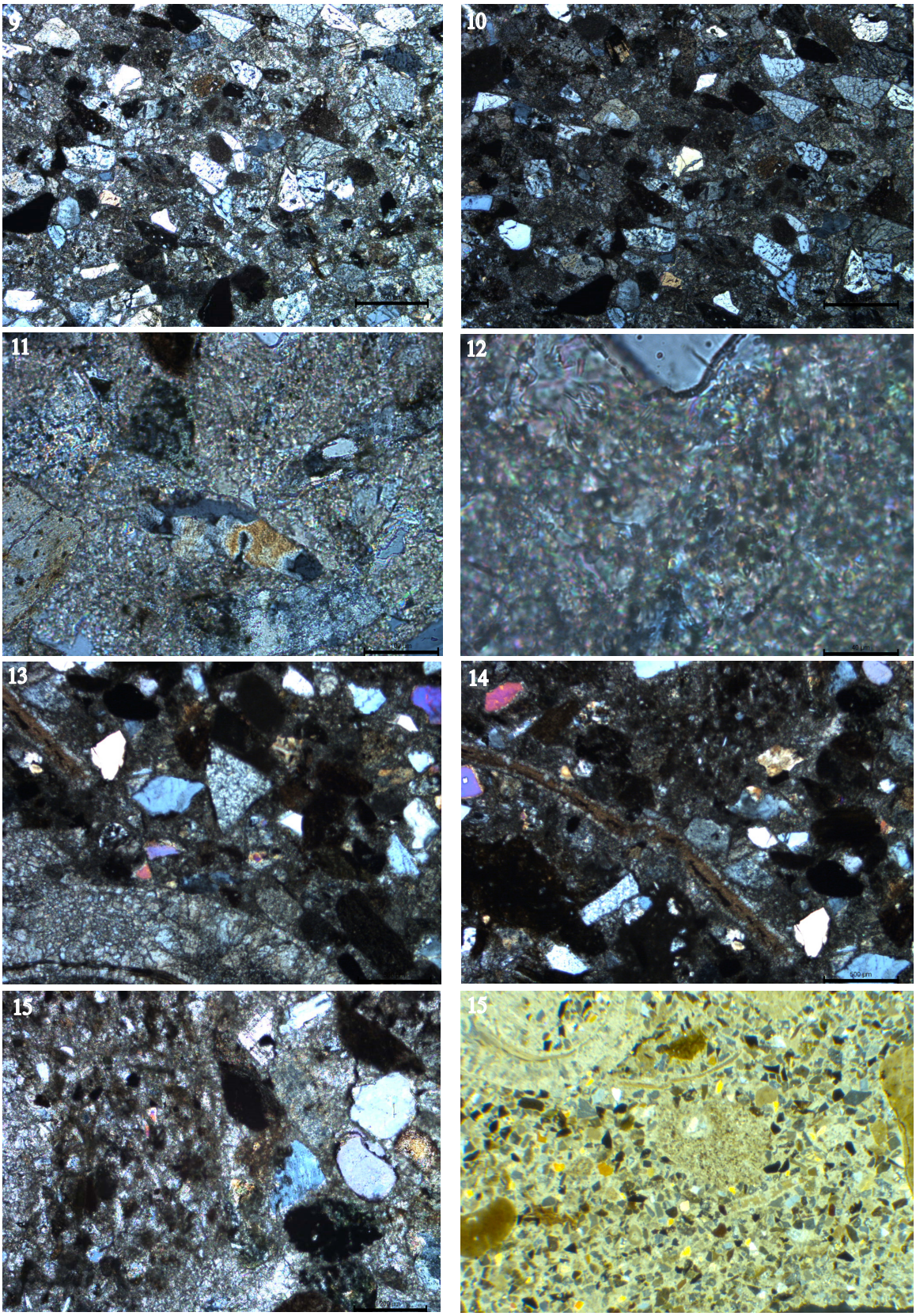

9-15) CDM bivalves and cements

APPENDIX 5

Slice	Location	Count	Total Area	Average Size	% Area
4370 N3					
IMG_0022	Center	2563	2.31E-04	9.02E-08	15.47
IMG_0021	Vug/Vein	1156	2.33E-04	2.02E-07	15.615
IMG_0020	Edge	3417	4.53E-04	1.33E-07	30.33
4370 N2					
IMG_0006	Edge	4059	0.003	6.44E-07	42.898
IMG_0014	Center	6278	0.001	2.36E-07	24.316
IMG_0013	Edge	2949	0.002	7.26E-07	35.141
IMG_0004	Vug/Vein	3369	9.24E-04	2.74E-07	15.166
IMG_0003	Edge	2144	0.003	1.20E-06	42.237
IMG_0002	Center	8143	0.002	2.59E-07	34.633
4370 N2 Middle					
IMG_0015	Center	6871	0.005	7.34E-07	21.336
IMG_0014	Center	5184	0.003	5.91E-07	12.957
4370 N2 Middle					
IMG_0017	Center	5869	5.27E-04	8.99E-08	34.865
IMG_0016	Center	6757	4.07E-04	6.02E-08	26.873
4389 N2 Rim					
IMG_0001	Edge	9198	0.002	2.19E-07	34.085
IMG_0002	Edge	8903	0.002	2.15E-07	32.527
4418 N1					
IMG_0025	Center	10434	0.002	1.71E-07	29.527
IMG_0024	Center	8956	0.001	1.65E-07	24.492
IMG_0023	Vug/Vein	2605	7.05E-04	2.71E-07	47.999
4418 N1 Rim					
IMG_0001	Edge	9198	0.002	2.19E-07	34.085
IMG_0002	Edge	8903	0.002	2.15E-07	32.527
4418 N3					
IMG_0029	Edge	598	0.002	2.85E-06	53.601
IMG_0028	Center	2735	0.004	1.63E-06	26.729
4445 N2					
IMG_0039	Edge	4481	0.007	1.53E-06	30.953
IMG_0039B	Edge	1782	0.001	7.27E-07	35.549
IMG_0038	Edge	4460	0.008	1.74E-06	35.023
IMG_0038BCROPMIDDLE	Center	1400	0.001	9.46E-07	45.297
IMG_0038BCROPEDGE	Edge	32	2.11E-04	6.59E-06	85.105
IMG_0037.JPG	All	3946	0.008	2.01E-06	35.75
IMG_0037BCROPMIDDLE	Center	654	5.39E-04	8.24E-07	32.49

IMG_0037BCROPEDGE	Edge	119	3.57E-04	3.00E-06	65.05
4445 N3					
IMG_0027	Edge	4356	0.01	2.28E-06	44.903
IMG_0027BCROPMIDDLE	Center	128	0.002	1.19E-05	93.494
IMG_0027BCROPRIGHT	Center	535	8.72E-05	1.63E-07	6.167
IMG_0026	Center	12908	0.002	1.78E-07	36.938
4776 N1					
IMG_0033	Center	6931	0.002	2.86E-07	31.93
IMG_0032	Vug/Vein	5842	5.20E-04	8.90E-08	35.627
IMG_0031	Vug/Vein	3480	5.43E-04	1.56E-07	37.184
4776 N2					
IMG_0036	All	4476	0.01	2.22E-06	41.902
IMG_0036BMIDCROP	Center	1134	0.001	1.29E-06	48.747
IMG_0036BEDGECROP	Edge	41	5.47E-04	1.33E-05	93.534
IMG_0035	All	1136	0.006	4.94E-06	23.675
IMG_0035BEDGECROP	Edge	21	2.71E-04	1.29E-05	86.127
IMG_0035BMIDCROP	Center	48	5.78E-05	1.20E-06	16.871
IMG_0034B	All	2027	0.014	7.14E-06	61.095
IMG_0034BMIDCROP	Center	917	7.67E-04	8.36E-07	35.984
IMG_0034BEDGECROP	Edge	39	7.54E-04	1.93E-05	89.885

Areas for nodules calculated in ImageJ

Slice	Location	Count	Total Area	Average Size	%Area
Bivalve Site BI3					
IMG_0043	Bivalve	4834	0.014	2.89E-06	58.712
IMG_0042	Bivalve	4773	0.014	2.91E-06	58.464
IMG_0041	Bivalve	4374	0.014	3.13E-06	57.577
Bivalve Site BI5					
IMG_0040	Bivalve	2323	0.012	5.37E-06	52.441
Bivalve Site Cement					
IMG_0016	Center	3189	0.002	7.20E-07	38.409
IMG_0016	Center	225	1.31E-04	5.80E-07	40.125
IMG_0015	Center	3530	0.002	6.87E-07	40.559
CDM Site BI3 Cement					
IMG_0019	Center	2584	0.001	5.43E-07	23.465
IMG_0018-1	Center	2718	0.002	8.97E-07	40.81
IMG_0017	Center	7012	3.27E-04	4.66E-08	22.546
CDM Site BI6					
IMG_0012	Center	4214	6.17E-04	1.47E-07	42.582

IMG_0011	Center	6833	4.71E-04	6.89E-08	32.474
IMG_0010	Center	6107	5.94E-04	9.73E-08	40.981
IMG_0009	Bivalve	6331	5.55E-04	8.76E-08	38.26
IMG_0008	Bivalve	5003	6.98E-04	1.40E-07	48.148
IMG_0007	Center	2395	6.78E-04	2.83E-07	46.748
CDM Site BI13/BI1					
IMG_0006	Center	6498	0.007	1.08E-06	27.015
CDM Site BI13-CO					
IMG_0008	Center	5264	9.27E-04	1.76E-07	65.799
CDM Site BI13-M1					
IMG_0001	Center	4182	0.009	2.16E-06	39.165
IMG_0002	Center	3296	0.01	3.12E-06	44.62
IMG_0003	Center	3407	0.01	2.79E-06	41.294
IMG_0004.JPG	Center	3376	0.009	2.77E-06	40.588
CDM Site BI16C2BI					
IMG_0024	Bivalve	10586	0.003	2.68E-07	46.752
CDM Site BI1C2C					
IMG_0021	Center	3090	0.003	9.37E-07	47.727
CDM Site BI16C2M					
IMG_0020	Center	3031	0.011	3.64E-06	45.267

Areas for bivalves and cements calculated in ImageJ